NEUROSCIENCE
RESEARCH ARTICLE

Andreas Lundt et al. / Neuroscience 409 (2019) 81–100

$Ca_v3.2$ T-Type Calcium Channels Are Physiologically Mandatory for the Auditory System

Andreas Lundt,[a] Robin Seidel,[b] Julien Soós,[a] Christina Henseler,[a] Ralf Müller,[c] Maheshwar Bakki,[a] Muhammad Imran Arshaad,[a] Dan Ehninger,[d] Jürgen Hescheler,[e] Agapios Sachinidis,[e] Karl Broich,[b] Carola Wormuth,[a] Anna Papazoglou[a] and Marco Weiergräber[a]*

[a]*Experimental Neuropsychopharmacology, Federal Institute for Drugs and Medical Devices (Bundesinstitut für Arzneimittel und Medizinprodukte, BfArM), Kurt-Georg-Kiesinger-Allee 3, 53175 Bonn, Germany*

[b]*Federal Institute for Drugs and Medical Devices (Bundesinstitut für Arzneimittel und Medizinprodukte, BfArM), Kurt-Georg-Kiesinger-Allee 3, 53175 Bonn, Germany*

[c]*Cognitive Neurophysiology, Department of Psychiatry and Psychotherapy and University Hospital Cologne, University of Cologne, Faculty of Medicine, Kerpener Str. 62, 50937 Cologne, Germany*

[d]*Molecular and Cellular Cognition, German Center for Neurodegenerative Diseases (Deutsches Zentrum für Neurodegenerative Erkrankungen, DZNE), Sigmund-Freud-Str. 27, 53127 Bonn, Germany*

[e]*Institute of Neurophysiology, University of Cologne, Faculty of Medicine, Robert-Koch-Str. 39, 50931 Cologne, Germany*

Abstract—Voltage-gated Ca^{2+} channels (VGCCs) play key roles in auditory perception and information processing within the inner ear and brainstem. Pharmacological inhibition of low voltage-activated (LVA) T-type Ca^{2+} channels is related to both age- and noise induced hearing loss in experimental animals and may represent a promising approach to the treatment of auditory impairment of various etiologies. Within the LVA Ca^{2+} channel subgroup, $Ca_v3.2$ is the most prominently expressed T-type channel entity in the cochlea and auditory brainstem. Thus, we performed a complete gender specific click and tone burst based auditory brainstem response (ABR) analysis of $Ca_v3.2^{+/-}$ and $Ca_v3.2^{-/-}$ mice, including i.a. temporal progression in hearing loss, amplitude growth function and wave latency analysis as well as a cochlear qPCR based evaluation of other VGCCs transcripts. Our results, based on a self-programmed automated wavelet approach, demonstrate that both heterozygous and $Ca_v3.2$ null mutant mice exhibit age-dependent increases in hearing thresholds at 5 months of age. In addition, complex alterations in W_{I-IV} amplitudes and latencies were detected that were not attributable to alterations in the expression of other VGCCs in the auditory tract. Our results clearly demonstrate the important physiological role of $Ca_v3.2$ VGCCs in the spatiotemporal organization of auditory processing in young adult mice and suggest potential pharmacological targets for interventions in the future.

Key words: auditory brainstem response, calcium channel, hair cells, spiral ganglion neuron, T-type, sensorineural hearing loss.

*Corresponding author. Tel.: +49 228 99307 4358; fax: +49 228 99307 3896.
E-mail address: Marco.Weiergraeber@bfarm.de (Marco Weiergräber).

Abbreviations: ABR, auditory brainstem response; AED, antiepileptic drug; AEP, auditory evoked potential; ARHL, age-related hearing loss; BERA, brainstem evoked response audiometry; BK, big conductance Ca^{2+}-activated K^+ channel; CWT, continuous wavelet transform; DHP, dihydropyridine; FFT, Fast Fourier Transformation; GT, genotype; HC, hair cell; HVA, high voltage-activated; IHC, inner hair cell; i.p., intraperitoneal; IWI, inter-wave-interval; LL, lateral leminiscus; LSO, lateral superior olive; LVA, low voltage-activated; NIHL, noise-induced hearing loss; OHC, outer hair cell; (q)PCR, quantitative polymerase chain reaction; RT, reverse transcription; SD, standard deviation; SEM, standard error of the mean; SGN, spiral ganglion neuron; SK, small conductance Ca^{2+}-activated K^+ channel; SNR, signal to noise ratio; SOC, superior olivary complex; SPL, sound pressure level; SPON, superior paraolivary nucleus; TWs, time windows; VGCC, voltage-gated Ca^{2+} channel.

INTRODUCTION

Loss of hair cells (HCs) and spiral ganglion neurons (SGN) is the major cause of age-related hearing loss (ARHL), i.e., presbycusis which normally affects high frequencies first (Schacht and Hawkins, 2005) and displays a prevalence of > 50 % in populations > 75 years of age (Gates and Mills, 2005). Calcium dyshomeostasis was proven to be of central relevance for age- and noise-related impairment of neuroacoustic function (Bao et al., 2005; Buchholz et al., 2007) with different types of voltage-gated Ca^{2+} channels (VGCCs) being expressed in inner and outer hair cells (OHCs and IHC, respectively), SGNs, the cochlear nucleus, the trapezoid body, the lateral superior olive (LSO) and

https://doi.org/10.1016/j.neuroscience.2019.04.024

further ascending components (Lopez et al., 2003; Lee et al., 2007; Shen et al., 2007; Nie et al., 2008; Simms and Zamponi, 2014; Zamponi, 2016, 2017). Based on electrophysiological and pharmacological properties, the pore-forming Ca_v-α_1 subunits of VGCCs complexes are subdivided into high voltage-activated (HVA), i.e., $Ca_v1.1$–1.4 L-type and $Ca_v2.1$–2.3 Non-L-type Ca^{2+} channels, and low voltage-activated (LVA) $Ca_v3.1$–3.3 T-type Ca^{2+} channels. The $Ca_v1.3$ VGCC was the first to be correlated with auditory dysfunction, as ablation of $Ca_v1.3$ in mice results in degeneration of IHCs and OHCs with subsequent deafness (Platzer et al., 2000; Glueckert et al., 2003). In addition, $Ca_v1.3$ was shown to be involved in the activity-dependent development of the auditory brainstem, evidenced by $Ca_v1.3$ deficient mice exhibiting a dramatic volume reduction in all auditory brainstem centers that occurred even before hearing onset (Hirtz et al., 2011). Thus, VGCC dysfunction can cause severe functional and developmental alterations in the peripheral auditory tract due to a highly complex and fine-tuned system of balanced Ca^{2+} influx that regulates spatiotemporal auditory processing.

Based on *in vitro* and *in vivo* findings on HC physiology, $Ca_v1.3$ VGCCs were originally considered potential candidates for the etiopathogenesis of ARHL and noise-induced hearing loss (NIHL) as well as targets for their prevention and therapy. Interestingly, age-related increases in brainstem-evoked response audiometry (BERA) thresholds turned out to be associated with a gradual decrease of $Ca_v1.3$ expression in IHC, OHC and the stria vascularis supporting a potential role for $Ca_v1.3$ in ARHL (Chen et al., 2013). Initially, it was suggested that only L-type VGCCs are involved in acoustic injury of the cochlea, as L-type blockers, e.g., diltiazem, verapamil and dihydropyridines (DHPs), but not T-type blockers such as mibefradil and flunarizine, seemed to decrease HC loss (Mills et al., 1999; Uemaetomari et al., 2009).

However, T-type VGCCs also exhibit complex spatiotemporal expression patterns in the auditory system, e.g., HCs (Inagaki et al., 2008), the cochlear nucleus (Kim and Trussell, 2007), the superior paraolivary nucleus (SPON) (Felix et al., 2011), and the LSO (Adam et al., 2001). Early immunohistochemical studies in 2 month old C57Bl/6 mice suggested weak $Ca_v3.1$ and $Ca_v3.3$, but no $Ca_v3.2$ VGCC expression in the organ of Corti. SGNs, however, exhibit dominant $Ca_v3.2$ with only moderate $Ca_v3.1$ and $Ca_v3.3$ expression (Shen et al., 2007). Whole cochlear qPCR in the same setting revealed highest transcript levels for $Ca_v3.2$ exceeding those for $Ca_v3.1$ and $Ca_v3.3$ by 2-fold and 100-fold, respectively (Shen et al., 2007). Additionally, no gender specific differences in expression levels were detected. Further quantification of T-type Ca^{2+} channels in the cochlea of young 6–8 wk old C57Bl/6J mice again revealed transcripts of all three T-type Ca^{2+} channels with $Ca_v3.2$ exhibiting the lowest expression (Yu et al., 2016). Lei et al. (2011) analyzed all three Ca_v3 T-type channel transcript levels in C57Bl/6 cochlea at 2, 4 and 8 months of age in which $Ca_v3.2$ levels clearly predominated and increased with age (Lei et al., 2011). This tendency was later confirmed for SGNs in C57Bl/6 mice aged 6–44 wk in which $Ca_v3.2$ transcripts also predominated (Yu et al., 2015). Thus Ca_v3 Ca^{2+} channels, particularly $Ca_v3.2$, display a complex developmental, i.e., spatiotemporal expression pattern within the cochlea.

Importantly, it was shown in 9–11 month old mice that ablation of $Ca_v3.2$ results in a significant delay of age-related loss of cochlear function and preservation of SGNs, further stressing a potential role for $Ca_v3.2$ in ARHL (Lei et al., 2011). Consequently, Ca^{2+} channel blockers and antiepileptic drugs (AEDs) known to inhibit T-type Ca^{2+} channels, e.g., trimethadione, ethosuximide, and flunarizine, were shown to preserve SGNs during aging (Mills et al., 1999; So et al., 2005; Shen et al., 2007; Lei et al., 2011). This prophylactic and therapeutic effect of AEDs that block T-type VGCCs was later also confirmed for NIHL (Bao et al., 2013; Yu et al., 2016) and it was suggested that multi-drug-multi-target therapeutic approaches including block of T-type VGCCs e.g., via ethosuximide (Gomora et al., 2001) and zonisamide (Matar et al., 2009) in combination with dexamethasone, could be a feasible approach for NIHL treatment as well (Bao et al., 2013). Notably, the positive effects of HC preservation and hearing threshold consolidation in ARHL and NIHL models seem to be age-dependent. Yu et al. (2016) reported that C57Bl/6 mice aged 24–26 wk did not experience any beneficial impact in hearing threshold at 8, 16, or 32 kHz upon mibefradil and benidipine administration. Even more important, histomorphological deterioration was detected in IHCs, e.g. stereocilia of IHCs were disorganized and sparse upon mibefradil administration. In addition, OHC loss was found upon benidipine application.

Given the potential role of $Ca_v3.2$ in ARHL and NIHL, we performed complete gender specific auditory profiling of young adult $Ca_v3.2^{+/-}$ and $Ca_v3.2^{-/-}$ mice, including click and tone burst related threshold characterization, amplitude growth function and latency analysis, as well as qPCR of cochlear VGCC transcripts, to unravel the physiological role of $Ca_v3.2$ VGCCs in the cochlea and the ascending auditory tract. Our results demonstrate for the first time that $Ca_v3.2$ VGCCs are of tremendous functional importance for spatiotemporal auditory processing in different areas of the auditory system and that pharmacological interference needs careful consideration based on both beneficial and adverse age-related effects.

EXPERIMENTAL PROCEDURES

Experimental animals

Controls, heterozygous and homozygous $Ca_v3.2$ deficient mice were generated from cryopreserved heterozygous embryos obtained via the Mutant Mouse Resource & Research Centers (MMRRC, supported by NIH). For further details, see MMRCC stock number 9979, strain name: B6.129-*Cacna1h*^{tm1Kcam}/Mmmh, strain of origin: C57BL/6 × 129, strain genetic background: C57BL/6 (Chen et al., 2003). Wild type littermates were used as controls.

Fifty-five animals were included in this study: 23 $Ca_v3.2^{+/+}$ mice (12 ♀, mean body weight: 24.09 g ± 0.41 g; 11 ♂, mean body weight: 32.82 g ± 0.58 g), 15 $Ca_v3.2^{+/-}$ mice (8 ♀, mean body weight: 23.50 g ± 0.41 g; 7 ♂, mean body weight: 33.11 g ± 0.81 g) and 17 $Ca_v3.2^{-/-}$ mice (8 ♀, mean body weight: 22.10 g ± 0.43 g; 9 ♂, mean body weight: 29.09 g ± 0.75 g). Gender-specific auditory brainstem response (ABR) audiometry was performed in mice aged 140.67 ± 0.38 days (~ 20 wk). All mice were housed in groups of 2–5 in clear Macrolon cages type II with *ad libitum* access to drinking water and standard food pellets. Using ventilated cabinets (Model 9AV125PYN, Techniplast, Germany; UniProtect, Zoonlab, Germany) as a noise-protected environment, mice were maintained at a temperature of 21 ± 2°C, 50–60 % relative humidity, and on a conventional 12 h light/dark cycle with a light onset at 5:00 a.m. Animals were strictly adapted to this circadian pattern for 14 days preceding subsequent experimentation.

All animal procedures were performed according to the guidelines of the German Council on Animal Care, and all protocols were approved by the local institutional and national committee on animal care (LANUV, Germany). The authors further certify that all animal experimentation was performed in accordance with the National Institute of Health Guide for the Care and Use of Laboratory Animals (NIH Publications No. 80–23) revised 1996 or the UK Animals (Scientific Procedures) Act 1986 and associated guidelines, or the European Communities Council Directive of 24 November 1986 (86/609/ EEC) and September 22nd, 2010 (2010/63/EU). Specific effort was made to minimize the number of animals used and their suffering.

Genotyping

$Ca_v3.2$ mutant mice were genotyped by PCR based on the protocol of the KAPA Mouse genotyping kit (Sigma Aldrich, Germany). The following primers were used: WT-forward: 5′-ATT CAA GGG CTT CCA CAG GGT A-3′, WT-reverse/ KO-forward: 5′-CAT CTC AGG GCC TCT GGA CCA C-3′, KO-reverse: 5′-GCT AAA GCG CAT GCT CCA GAC TG -3′ (see also Chen et al., 2003). PCRs were performed using a C1000 thermal cycler (BioRad, Germany) with initial denaturation (95°C – 1 min), followed by 35 cycles (denaturation 95°C – 15 sec, annealing 61°C – 15 sec, extension 72°C – 1 min) and final extension (72°C – 10 min). Subsequently, PCR products were separated via agarose gel electrophoresis and detected by ChemiDoc Touch (BioRad, Germany) (Fig. 1).

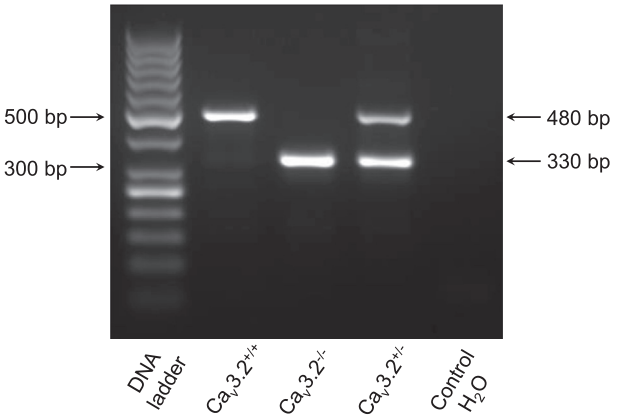

Fig. 1. Genotyping of $Ca_v3.2$ mutant mice. $Ca_v3.2^{+/+}$, $Ca_v3.2^{+/-}$ and $Ca_v3.2^{-/-}$ mice were generated from cryopreserved heterozygous embryos. Chromosomal DNA was extracted from tail biopsies of the offspring for subsequent genotyping. Amplification in $Ca_v3.2^{+/+}$ results in a 480 bp fragment and a 330 bp fragment in $Ca_v3.2$ deficient ($Ca_v3.2^{-/-}$) mice. In heterozygous $Ca_v3.2^{+/-}$ mice, both fragments are detected (see also (Chen et al., 2003).

ABR recording procedure

Prior to ABR recordings, animals were anesthetized using intraperitoneal (i.p.) injection of ketamine (100 mg/kg body weight, Ketanest® S, 25 mg/ml Pfizer, Germany) and xylazine (10 mg/kg body weight, Rompun® 2%, Bayer, Germany) and placed inside a sound attenuating cubicle (ENV-018V, Med Association, Inc., USA) lined with an acoustic foam. The entire cubicle was covered with a custom made meshed metal Faraday cage (stainless steel, 2 mm thickness, 1 cm mesh size) to shield ABR recordings from external electrical interference and to protect from noise. Following anesthesia, animals were placed on a homeothermic heating blanket (ThermoLux®, Witte + Sutor, Murrhardt, Germany) inside the attenuating cubicle to maintain core body temperature. Eyes were covered with an eye ointment (5 % Dexpanthenol, Bepanthen®, Bayer Vital GmbH, Germany) to protect against corneal desiccation.

For recording of monaural bioelectrical auditory potentials, subdermal stainless steel electrodes (27GA 12 mm, Rochester Electro-Medical, USA) were inserted at the vertex, axial to the pinnae (positive (+) electrode) and ventrolateral to the right pinna (negative (-) electrode) (Fig. 2). The ground electrode was positioned at the hip of the animal. Impedance measurements of all electrodes were performed prior to each recording to verify proper electrode positioning / conductivity and were set < 5 kΩ. All ABR recordings were performed under free field conditions using a single loudspeaker (MF1 Multi-Function Speaker, Tucker-Davis Technologies, TDT, USA) placed 10 cm opposite the rostrum of the animals (loudspeaker leading edge perpendicular to the mouse interaural axis). Stimulus protocols for click and tone bursts were programmed using SigGenRZ software (Tucker-Davis Technologies, TDT, USA). The resultant bioelectrical signals recorded from the subdermal electrodes were transferred to a head stage (RA4LI, Tucker-Davis Technologies, TDT, USA) and further forwarded to the preamplifier (RA4PA, Tucker-Davis Technologies, TDT, USA) with 20-fold amplification. Acoustic stimulus presentation, equipment, e.g., loudspeaker control, ABR acquisition, processing, averaging and data management, were further coordinated using the RZ6 Multi I/O Processor system and BioSigRZ software (both Tucker-Davis Technologies, TDT, USA).

ABR data acquisition was performed at a sampling rate of 24.4 kHz, and signals were bandpass filtered (high pass 300 Hz, low pass 5 kHz) using a 6-pole Butterworth filter. Individual ABR data acquisition time was 25 ms, starting

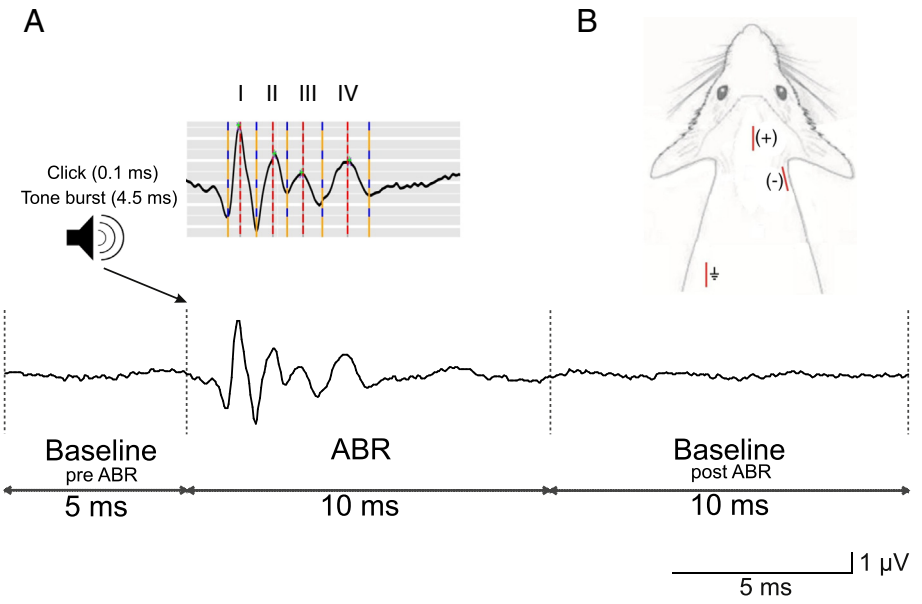

Fig. 2. ABR analysis and ABR electrode position. **A)** An individual ABR recorded at 65 dB SPL. An initial pre-stimulus 5 ms baseline (pre-stimulus TW_1) was followed by a transient acoustic stimulus (e.g., click, 100 µs duration; tone burst, 4.5 ms duration). Ten ms after stimulus onset, another 10 ms baseline (post-stimulus TW_2) was recorded. Both baseline recordings (TW_1 + TW_2) were used to calculate the SD of baseline noise. The hearing threshold was reached whenever an individual ABR wave amplitude (labelled by Roman numerals I–IV) exceeded fourfold the SD of baseline noise. For wave amplitude and wave latency comparison, a "Mexican hat" based wavelet analysis was performed that automatically characterized negative peaks (blue-yellow striped lines) and positive peaks (red-grey striped lines) within the recorded ABR, thereby determining the temporal frames of $W_{I\text{-}IV}$. Green crosses indicate maximum ABR wave amplitudes. Note that these maxima represent nominal values and do not indicate approximated values based on the "Mexican hat" based wavelet approach. **B)** For monaural based ABR recordings, subdermal stainless steel electrodes were used. The reference electrode was positioned at the left hip, the positive electrode (+) was placed at the vertex (axial the pinnae) and the negative electrode (-) was located ventrolateral of the right pinna.

with a 5 ms baseline period prior to the individual acoustic stimulus onset (pre ABR baseline) and exceeding the 10 ms ABR section by another 10 ms baseline (post ABR baseline, Fig. 2).

Two types of acoustic stimuli were used in this study and were generated using SigGenRZ software (Tucker-Davis Technologies, TDT, USA) and applied via the TDT BioSigRZ platform. The first stimulus entity was a 100 µs duration click with alternating polarity (switching between condensation and rarefaction) (Tucker-Davis Technologies, 2015). This stimulus was used to analyze and determine click thresholds, ABR wave I–IV amplitudes and wave I–IV latencies. The second stimulus entity was a 4.5 ms tone burst (transient sinusoidal pulse) of alternating polarity with Hann window for rise and fall times of 1.5 ms duration. This stimulus was used to analyze and identify frequency specific hearing thresholds in all genotypes. The frequency range was studied from 1–42 kHz in 6 kHz steps. All acoustic stimuli were applied 300 times at a rate of 20 Hz and averaged. For ABR threshold recordings, sound pressure levels (SPL) were increased in 5 dB steps for clicks and 10 dB steps for tone bursts (Willott, 2001; Scimemi et al., 2014; Rotschafer et al., 2015; Tucker-Davis Technologies, 2015), starting from 0 dB up to 90 dB (increasing SPL mode). Note that SPLs for tone bursts within the range of 1–42 kHz were calibrated each day prior to recording using a microphone (378C01, PCB Piezotronics, NY, USA) connected to a preamplifier (480C02, PCB Piezotronics) and the RZ6 Multi I/O Processor system (Tucker-Davis Technologies, TDT, USA). The microphone was positioned inside the sound attenuating cubicle to mimic the experimental murine ear and connected to an oscilloscope (DPO3012, Tektronix, USA) to monitor and confirm the spectrum of sound stimuli using online Fast Fourier Transformation (FFT).

ABR analysis – general aspects and software

To avoid potential inconsistencies in ABR threshold determination by visual inspection/estimation, we performed automated threshold detection based on earlier publications (Bogaerts et al., 2009; Probst et al., 2013; Alvarado et al., 2014). For data processing and analysis, "R" software (The R Foundation, version 3.2.1, R Core Team 2015) was used with additional packages, including "reshape2" (version 1.4.1), "ggplot2" (version 1.0.1), "data.table" (version 1.9.4), "gdata" (version 2.13.3), "pastecs" (version 1.3.18), "waveslim" (version 1.7.5) and "MassSpecWavelet" (version 1.30.0; (Du et al., 2006). Wavelet analysis was performed using the "MassSpecWavelet" package (Du et al., 2006).

Analysis of hearing thresholds

To determine the click and tone burst derived thresholds of ABR recordings, three distinct time windows (TWs) were set to calculate the signal to noise ratio (SNR), i.e., TW_1 (pre stimulus, 0–5 ms), TW_2 (stimulus related, 5–15 ms) and TW_3 (post stimulus, 15–25 ms). Noise standard deviation of the baseline was calculated within two distinct TWs, i.e., TW1 and TW3 where no auditory evoked potentials (AEP) were observed (Fig. 2A). For each SPL measurement within an ABR record setting both mean and standard deviation were calculated for pooled TW_1 and TW_3 data. Subsequently, all recording samples were reset individually by the corresponding calculated mean. The threshold of hearing (TH) was determined by the lowest SPL (dB) where at least one wave amplitude (A) value (W_I–W_{IV}) in the ABR response time window (TW_2) exceeded fourfold of the previously calculated standard deviation ($T_{[SPL\ (dB)]}$: $A_{WI\text{-}IV(TW2)} > 4 \times SD_{(TW1,TW3)}$). If no ABR wave (I–IV) was detected for frequency threshold

analysis at maximum SPL, a nominal threshold level of 100 dB was assigned.

ABR wave amplitude and wave latency analysis

To determine the temporal collocation of all positive (p) waves (peaks, see intercept points of red-grey lines with ABR trace) as well as negative (n) waves (pits, see intercept points of blue-orange lines with ABR trace, Fig. 2A), a "Mexican hat" wavelet based analysis was conducted which uses a default wavelet by the continuous wavelet transform (CWT)-based pattern-matching algorithm (Du et al., 2006). Mathematically, the CWT is represented as (Daubechies, 1992), see also (Valderrama et al., 2014):

$$C(a,b) = \int_R s(t)_{a,b}\,(t)\,dt,\ {}_{a,b}(t)$$
$$= \frac{1}{\sqrt{a}}\left(\frac{t-b}{a}\right),\ a \in R^{+} - \{0\},\ b \in R,$$

where *s(t)* is the signal, *a* is the scale, *b* is the translation, *ψ(t)* is the mother wavelet, $\psi_{a,b}(t)$ is the scaled and translated wavelet and *C* is the 2D matrix of wavelet coefficients.

In an initial step, a 65 dB measurement of each ABR run was used to identify the best scale parameters for each wave to be passed to the CWT, resulting in three classes: scale parameters 0.5–4 for all n-waves, 0.5–6 for all p-waves and 0.5–12 for wave IV, as this was the broadest wave within the samples. All classes proved to reliably detect the correct temporal collocation of waves I–IV within all 65 dB measurements.

To determine ABR waves I–IV in the accurate temporal sequence at 65 dB SPL, p-peaks (Fig. 2A, red-grey lines) and n-peaks (pits, Fig. 2A, yellow-blue lines) were identified in a fixed progression using relative positions of previously identified peaks to limit the TW of subsequent scans. Once all nine peaks had been characterized at 65 dB (Fig. 2A), these values were used as references (starting points) for the temporal search frame for adjacent sound pressure measurements (60 dB and 70 dB) before identification of peaks 1–9 was reinitiated. Accordingly, p- and n-peaks for all dB SPLs (65–0 dB and 70–90 dB) were determined if possible. Once a p- and n-peak were no longer identifiable by wavelet analysis, their temporal collocation was set by calculating the temporal offset of the peak to any other peak identified in the previous dB level. Applying the temporal offset of peaks to any other p- and n-peak within the current dB level resulted in a maximum of eight determined temporal positions for the undefined peaks in which the mean was taken as the closest approximation.

To evaluate amplitude growth function and latency comparison of all waves ($W_{I\text{-}IV}$), maximum amplitudes (Fig. 2A, green crosses) and mean latencies (Fig. 2A, red-grey lines) of each of the four p-peaks within the time frame of the related n-peaks were further evaluated. Importantly, all results based on the self-programmed automatic wavelet tool were subsequently visually confirmed based on an independent, blinded manual ABR analysis performed by a different investigator. In rare cases, individual ABR runs were excluded from statistics due to, for example, noise contamination. Note that our approach determines "Mexican hat" wavelet based time frames of each wave ($W_{I\text{-}IV}$) for subsequent identification of the actual maxima and related latencies. This is similar to a recent study by Valderrama et al. (2014) that applies a "Mexican hat" based fitted parametric peaks (FPP) approach using synthesized peaks (Valderrama et al., 2014).

Real time PCR of $Ca_v3.2$ transgenic mouse cochlea

qPCR was performed in $Ca_v3.2^{+/+}$, $Ca_v3.2^{+/-}$ and $Ca_v3.2^{-/-}$ mice to identify potential alterations in cochlear transcript levels of other VGCCs, i.e., HVA L-type $Ca_v1.2$ and $Ca_v1.3$, HVA Non L-type $Ca_v2.3$, LVA T-type $Ca_v3.1$ and $Ca_v3.3$, that are known to be expressed within the cochlea and the auditory tract. For each genotype, the following gender specific subgroups were used for analysis: $Ca_v3.2^{+/+}$: ♀, n = 8, 21.27 ± 0.38 wk; ♂, n = 8, 21.23 ± 0.41 wk; $Ca_v3.2^{+/-}$: ♀, n = 8, 21.32 ± 0.40 wk; ♂, n = 8, 21.04 ± 0.31 wk; $Ca_v3.2^{-/-}$: ♀, n = 8, 21.41 ± 0.21 wk; and ♂, n = 8, 20.98 ± 0.21 wk. Note that experimental animals for cochlear qPCR analysis were not involved in ABR experiments to eliminate potential confounding factors.

Both cochleae of each individual animal were dissected in an RNase free environment (RNAlater® stabilization reagent, Qiagen, Germany) and snap-frozen in liquid nitrogen. Total RNA from both mouse cochleae was extracted using Direct-zol™ RNA Micro Kit (Zymo Research, Freiburg i.Br., Germany) followed by an additional step of DNase digestion (Turbo DNA-free™ Kit, Ambion®, Thermo Fisher Scientific; Germany). Quality and quantity of total RNA was evaluated using Nanodrop standard procedures (Nanodrop™ 1000, Thermo Fisher Scientific, Germany). cDNA synthesis was performed via a two-step RT-PCR approach using both random hexamer and anchored-oligo$(dt)_{18}$ primers with 250 ng total cochlear RNA from each animal for the final 50 µl first-strand cDNA mix (Transcriptor First-Strand cDNA synthesis Kit, Roche, Germany). cDNA (2 µl) served as a template for qPCR (see below), and signal detection was based on SYBR Green I Master (Roche, Germany). qPCR experiments were carried out using a LightCycler 480 System (Roche, Germany) with the following protocol (per cycle) being applied for all primer pairs (Table 1): 95°C (10 min, pre-incubation step); 95°C (10 s, denaturation step); 60°C (20 s, annealing step); 72°C (30 s, extension step). Forty total cycles were performed.

Every cochlea sample was tested in triplicate, and two negative controls were added in duplicate, (no template; no RT) for the qPCR 96-well-plate (Roche, Germany). Furthermore, to avoid inter-run variations and ensure statistical comparability among the plates, cochlea cDNA derived from C57Bl6/J mice served as a positive control and calibrator cDNA and was also used in triplicate on every plate. Amplification specificity was verified by melting curve analysis (LightCycler480 System Software, Roche). Deionized, nuclease-free water (no cDNA) and total RNA samples (without RT) were used as controls, and HPRT was utilized

Table 1. Sequence of primer pairs used for qPCR (OriGene Technologies [(a)]; Weiergräber et al., 2005 [(b)]).

Gene	Protein	Forward sequence (5′–3′)	Reverse sequence (5′–3′)
Cacna1c [a]	$Ca_v1.2$ α_1	CGTTCTCATCCTGCTCAACACC	GAGCTTCAGGATCATCTCCACTG
Cacna1d [a]	$Ca_v1.3$ α_1	CTACCGTTGCACAGATGAAGCC	TCACGGACCACAGGACTGTCAA
Cacna1e [a]	$Ca_v2.3$ α_1	ATGGACAAGGCTACCACGGAGA	GACTGGCTTCTCCATCCGTCTT
Cacna1g [a]	$Ca_v3.1$ α_1	GACCATGTGGTCCTCGTCATCA	TTTCAGCCAGGAAGACTGCCGT
Cacna1i [a]	$Ca_v3.3$ α_1	GTCTTCACCAAGATGGACGACC	ACTTCGCACCAGTCAGGCTTGT
Hprt [b]	HPRT	GCTGGTGAAAAGGACCTCT	CACAGGACTAGAACACCTGC

as an internal reference gene. Ct-values (cycle threshold) were calculated using the LightCycler 480 System software (Roche).

Individual primer efficiency, analysis and qPCR statistics were performed using qBase+ qPCR analysis software (Biogazelle, Gent, Belgium) which is based on a delta-Cq quantification model with PCR efficiency correction, reference gene normalization and inter-run calibration (Hellemans et al., 2007). All results were determined as CNRQ (Calibrated Normalized Relative Quantity) and statistically analyzed using the Mann-Whitney test.

Statistical analysis

All results in this study are presented as group means ± SEM using GraphPad Prism 6 software (V6.07 GraphPad Software, Inc., USA). Both genders were analyzed separately. Significant differences were compared using an ordinary one-way ANOVA for click-evoked hearing threshold analysis (Fig. 8) and latency analysis for each single wave (Fig. 12) followed by Tukey's multiple comparisons test. Two-way repeated measure ANOVA followed by Tukey's adjustment for multiple comparisons was performed to evaluate differences in tone burst evoked hearing thresholds (Fig. 10) and to calculate differences in amplitude growth function (Fig. 11). qPCR results were statistically analyzed using the Mann-Whitney test. Statistical significance was determined using α-level = .05 and *P*-values defined as $^*P < .05$; $^{**}P < .01$; $^{***}P < .001$; and $^{****}P < .0001$. Note that asterisks indicate significant differences between controls and transgenic animals ($Ca_v2.3^{-/-}$ and $Ca_v3.2^{+/-}$) whereas "+" icons represent significant differences between $Ca_v3.2^{+/-}$ and $Ca_v3.2^{-/-}$.

RESULTS

Developmental alterations in $Ca_v3.2$ transgenic mice

The α1H knockout ($Ca_v3.2^{-/-}$) mouse model exhibits cardiac pathology (Chen et al., 2003), which is of particular significance as cardiovascular disease can promote hearing loss (Gates et al., 1993). Given the partially controversial results on the $Ca_v3.2$ null mutant phenotype, we first unraveled potential developmental alterations in body weight in female and male controls (♀, n = 12; ♂, n = 11), $Ca_v2.3^{+/-}$ (♀, n = 8; ♂, n = 7) and $Ca_v2.3^{-/-}$ (♀, n = 8; ♂, n = 9) mice aged 140.67 ± 0.38 days. In females, a significant decrease in body weight was observed for $Ca_v3.2^{-/-}$ mice compared to controls (Fig. 3). In males, $Ca_v3.2^{-/-}$ mice exhibited a significant weight reduction compared to $Ca_v3.2^{+/+}$ mice and $Ca_v3.2^{+/-}$ mice (Fig. 3A). In heterozygous mice, which do not display cardiac pathology (Chen et al., 2003), no alterations were observed in body weight compared to controls at 20 wk of age. Long-time body weight monitoring revealed reduced weight in female $Ca_v3.2^{+/-}$ and $Ca_v3.2^{-/-}$ mice with increased age (> 25 wk, Fig. 3B), and the same held true for male $Ca_v3.2$ null mutants (Fig. 3C).

Click and tone burst evoked ABRs in control, $Ca_v3.2^{+/-}$ and $Ca_v3.2^{-/-}$ mice

To elucidate the role of $Ca_v3.2$ VGCCs in auditory processing, we performed click and tone burst evoked ABR recordings to evaluate hearing threshold differences, amplitude growth function and latency comparison in $Ca_v3.2^{+/+}$ mice (controls) and $Ca_v3.2^{+/-}$ and $Ca_v2.3$ null mutant mice ($Ca_v3.2^{-/-}$). Specific emphasis was placed on the evaluation of both genders, as gender-specific differences in auditory parameters and ARHL have been reported in both human (Pearson et al., 1995; Murphy and Gates, 1997) and mouse (Henry, 2004; Ison et al., 2007). ABRs to free field click (0.1 ms) and tone burst (1–42 kHz in 6 kHz steps, 4.5 ms in total with a 1.5 ms ramp time) acoustic stimuli were recorded using subdermal electrodes (for electrode positioning see *Experimental Procedures*). Note that vertex positive potentials are plotted as upward deflections as depicted in representative click-evoked recordings for female $Ca_v3.2^{+/+}$ (Fig. 4A), $Ca_v3.2^{+/-}$ (Fig. 4B) and $Ca_v3.2^{-/-}$ mice (Fig. 4C). Representative ABR recordings in females suggests increased click evoked ABR thresholds and reduced amplitude growth function (for details see below). Similarly, representative ABR recordings in males suggested increased click evoked ABR thresholds and reduced amplitudes in $Ca_v2.3^{-/-}$ (Fig. 5C) compared to control (Fig. 5A) and heterozygous $Ca_v3.2^{+/-}$ mice (Fig. 5B, for details see below). Representative tone burst evoked ABRs are depicted in Fig. 6A-C for females and in Fig. 7A-C for males. Note that representative ABR recordings suggest frequency specific hearing loss in the higher frequency range and reduced amplitude in both $Ca_v3.2^{+/-}$ (Figs. 6B, 7B) and $Ca_v3.2^{-/-}$ mice (Figs. 6C, 7C).

Click related hearing thresholds in controls, $Ca_v3.2^{+/-}$ and $Ca_v3.2^{-/-}$ mice

To evaluate the effect of $Ca_v3.2$ allelic loss on general hearing performance, we analyzed click evoked ABRs for different SPLs (0–90 dB) in all three genotypes aged 140.67 ± 0.38 days. Using our automated ABR threshold detection system, a significant difference in hearing threshold among the

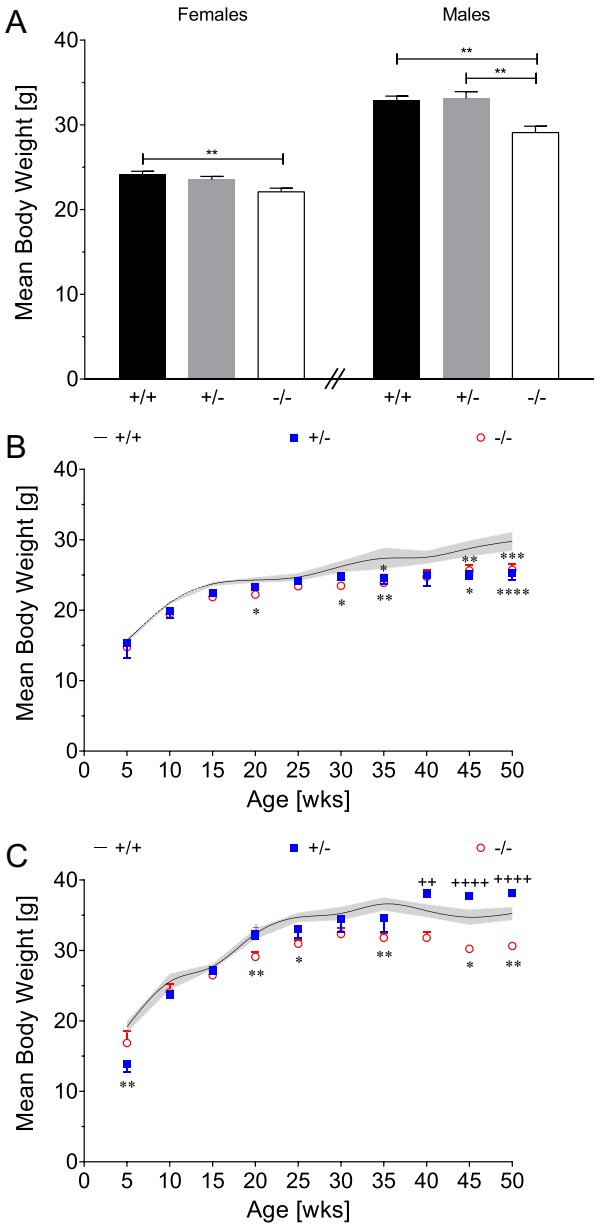

Fig. 3. Body weight in $Ca_v3.2^{+/+}$, $Ca_v3.2^{+/-}$ and $Ca_v3.2^{-/-}$ mice. **A**) Body weight of $Ca_v3.2^{+/+}$ (♀, n = 12; ♂, n = 11), $Ca_v3.2^{+/-}$ (♀, n = 8; ♂, n = 7) and $Ca_v3.2^{-/-}$ (♀, n = 8; ♂, n = 9) mice was evaluated age 140.67 ± 0.38 days. A significant decrease in body weight was observed for female $Ca_v3.2^{-/-}$ mice compared to controls (22.10 ± 0.43 g vs. 24.09 ± 0.41 g, $P < .01$). Male $Ca_v3.2^{-/-}$ mice displayed a significantly reduced body weight compared to both $Ca_v3.2^{+/+}$ (29.09 ± 0.75 g vs. 32.82 ± 0.58 g, $P < .01$) and $Ca_v3.2^{+/-}$ animals (29.09 ± 0.75 g vs. 33.11 ± 0.81 g, $P < .01$). In heterozygous mice no alterations were observed compared to controls. **B, C**) Body weight development was monitored for controls (-), $Ca_v3.2^{+/-}$ (■) and $Ca_v3.2^{-/-}$ mice (○) from 5 to 50 wk of age. Control values were used to generate a fitted curve (black line) with the 95% confidence interval in grey. Note that in females, a significant reduction in body weight was observed in $Ca_v3.2^{+/-}$ and $Ca_v3.2^{-/-}$ mice (**B**). The same held true for male $Ca_v3.2^{-/-}$ mice (**C**). Ordinary one-way ANOVA followed by Tukey's multiple comparisons test was used to perform statistical analysis. The results are presented as the mean ± SEM.

genotypes was detected. $Ca_v3.2^{-/-}$ mice exhibited a significant increase of hearing threshold compared to $Ca_v3.2^{+/+}$ controls (Fig. 8A, B). The same held true in comparison to $Ca_v3.2^{+/-}$ mice (Fig. 8A, B). Note that no gender specific alterations were observed in hearing thresholds within individual genotypes ($Ca_v3.2^{+/+}$, $Ca_v3.2^{+/-}$ and $Ca_v3.2^{-/-}$) at the age of 20 wk.

At the age of 40 wk (280.72 ± 0.60 days), hearing thresholds significantly increased in $Ca_v3.2^{-/-}$ mice compared to controls in both genders (Fig. 9). In males, the hearing threshold of α1H null mutant mice also exceeded the threshold of $Ca_v3.2^{+/-}$ mice (Fig. 9). Note that no gender specific differences within the three individual genotypes ($Ca_v3.2^{+/+}$, $Ca_v3.2^{+/-}$ and $Ca_v3.2^{-/-}$) were detected at the age of 40 wk.

The effect of aging on progressive hearing loss, i.e., increased hearing threshold, was analyzed in animals at 20 and 40 wk of age. In females, controls and $Ca_v3.2^{+/-}$ mice exhibited a significant increase in hearing threshold between 20 and 40 wk ($P < 0.01$), whereas $Ca_v3.2^{-/-}$ mice displayed a trend ($P = .079$). In males, no significant increase in hearing threshold was detected for controls or heterozygous mice from 20 to 40 wk of age ($P = .136$ and $P = .057$, respectively). In male $Ca_v3.2^{-/-}$ mice however, a clear age-related increase in hearing loss was observed ($P < .0001$) (Figs. 8, 9).

Tone burst related hearing thresholds in controls, $Ca_v3.2^{+/-}$ and $Ca_v3.2^{-/-}$ mice

To determine potential alterations in ABR threshold levels evoked by different tone burst frequencies (1–42 kHz, Fig. 10A, B), we performed repeated two-way ANOVA followed by Tukey's multiple comparisons test. Significant interaction was observed for males regarding GT and stimulus frequency, whereas no significant interaction could be confirmed in female mice. Highly significant effects were observed for a GT effect and tested frequency on threshold levels. Multiple comparisons revealed significant differences for various stimulus frequencies within the frequency range of 6–36 kHz in both $Ca_v3.2^{-/-}$ female and male mice (Fig. 10A, B).

The percentage of animals with detectable hearing thresholds for the individual frequencies is displayed in Fig. 10C, D. Unpaired two-way ANOVA revealed a significant interaction between GT and frequency for male mice, no significant interaction for female mice and high significant effects of GT and tested frequency. $Ca_v3.2^{-/-}$ mice from both genders exhibited significantly reduced hearing ability for lower (1 kHz for female mice) and higher frequencies (females: 30–42 kHz; males: 24–42 kHz) compared to $Ca_v3.2^{+/+}$ and $Ca_v3.2^{+/-}$ animals based on Tukey´s multiple comparisons test (Fig. 10C, D).

Click-evoked ABR amplitude growth function analysis

In response to moderate to high -intensity clicks there may occur up to seven ABR peaks (W_I–W_{VII}) that are related to the following neuroanatomical structures: W_I, auditory nerve (distal portion, within the inner ear); W_{II}, cochlear nucleus (proximal portion of the auditory nerve, brainstem

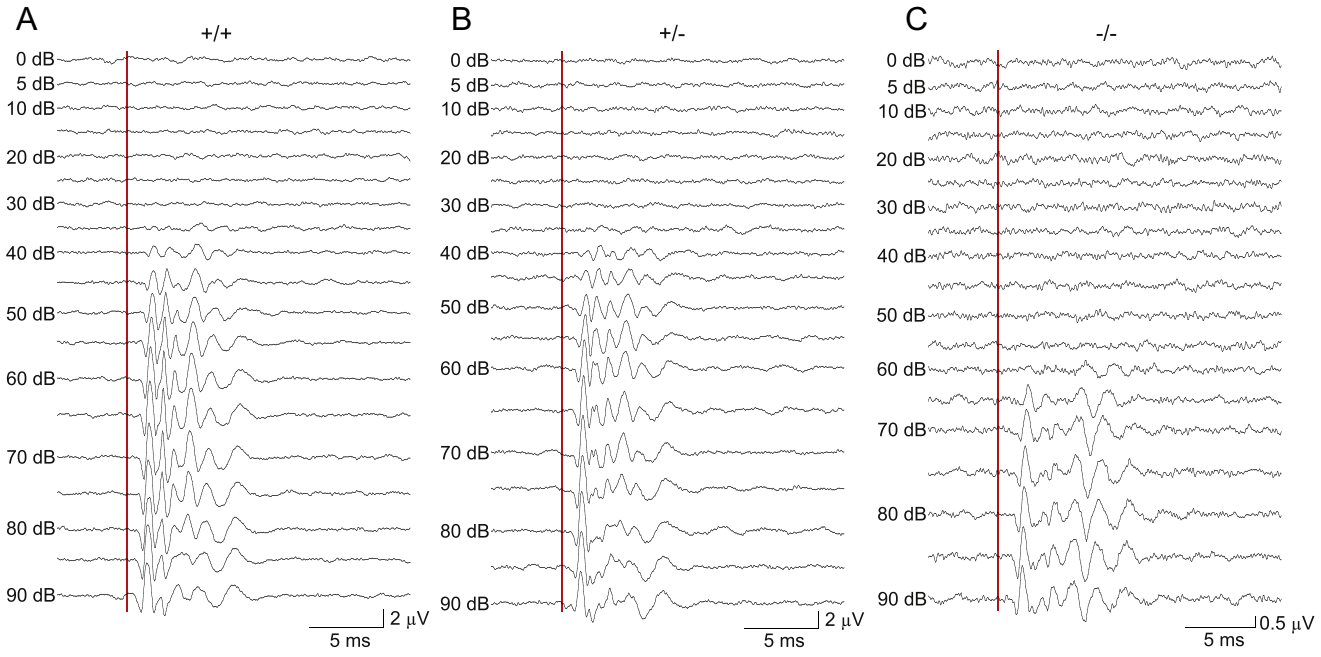

Fig. 4. Click based ABRs in female $Ca_v3.2$ transgenic mice. Representative ABRs obtained from $Ca_v3.2^{+/+}$ (**A**), $Ca_v3.2^{+/-}$ (**B**) and $Ca_v3.2^{-/-}$ (**C**) female mice (aged 140.67 ± 0.38 days) upon click stimulation (increasing SPL (dB) from 0–90 dB with 5 dB SPL steps). Each stimulus entity was presented 300 times at 20 Hz and averaged. The red line indicates the onset of the acoustic stimulus. Note that the ABR wave amplitudes are reduced in female $Ca_v3.2^{-/-}$ mice (y-axis scaling has been adapted accordingly in (**C**)).

termination); W_{III}, superior olivary complex (SOC); W_{IV}, lateral leminiscus (LL); W_V, termination of the lateral leminiscus (LL) within the inferior colliculus (IC) on the contralateral side (Knipper et al., 2013). It should be noted that waves II–V are likely to have more than one anatomical structure of the ascending auditory pathway contributing to them.

In 51.0 % of all click evoked ABR recordings, we identified five distinct positive waves at an SPL of 65 dB. In 25.4% of all recordings, we detected six distinct waves, and in 23.6% of all recordings, the number of identified distinct waves was limited to four within the first 10 ms at 65 dB SPL. Based on these findings, we focused our analysis on $W_{I\text{-}IV}$.

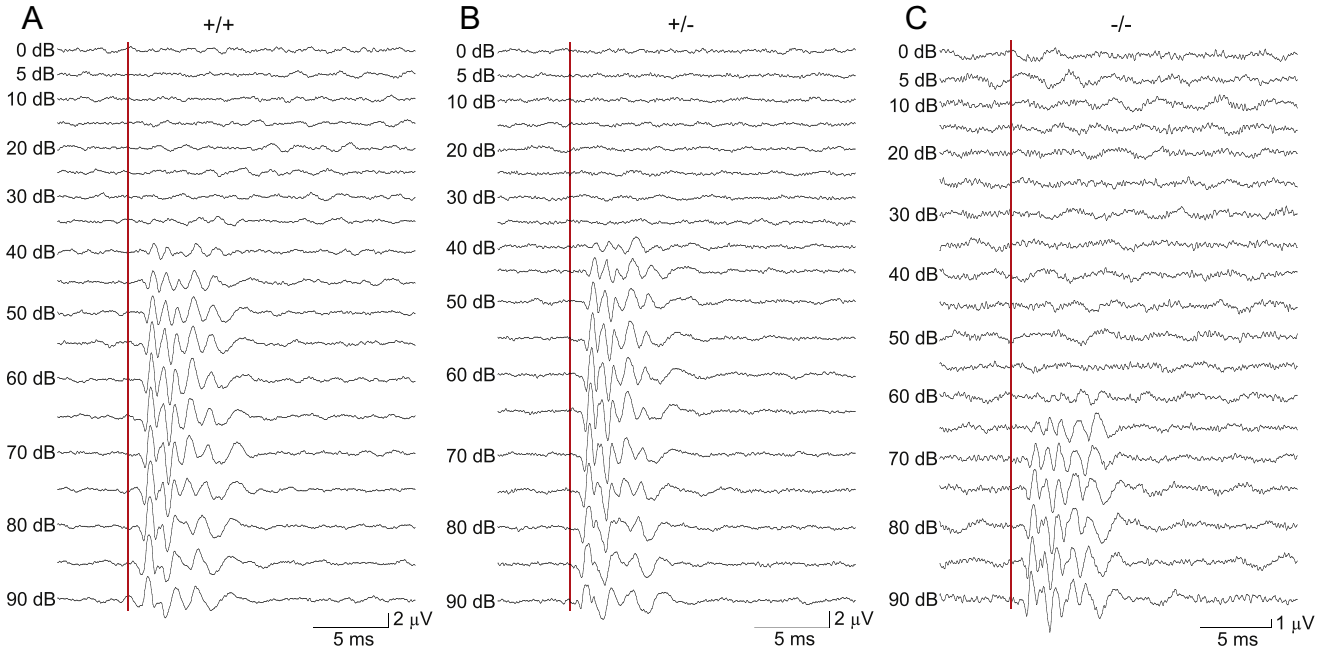

Fig. 5. Click based ABRs in male $Ca_v3.2$ transgenic mice. Representative ABRs obtained from $Ca_v3.2^{+/+}$ (**A**), $Ca_v3.2^{+/-}$ (**B**) and $Ca_v3.2^{-/-}$ (**C**) male mice (aged 140.67 ± 0.38 days) upon click stimulation (increasing SPL (dB) from 0–90 dB with 5 dB SPL steps). Each stimulus entity was presented 300 times at 20 Hz and averaged. The red line indicates the onset of the acoustic stimulus. Note that the ABR wave amplitudes are reduced in male $Ca_v3.2^{-/-}$ mice (y-axis scaling has been adapted accordingly in (**C**)).

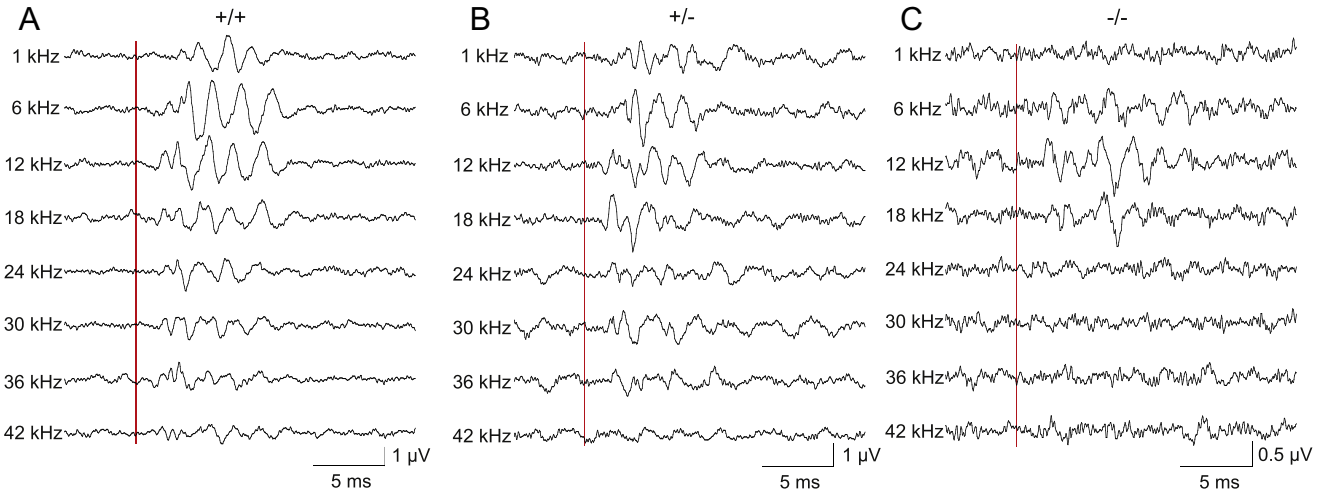

Fig. 6. Tone burst evoked ABRs in female $Ca_v3.2$ transgenic mice. Representative ABRs from $Ca_v3.2^{+/+}$ (**A**), $Ca_v3.2^{+/-}$ (**B**) and $Ca_v3.2^{-/-}$ (**C**) female mice (aged 140.67 ± 0.38 days) following tone bursts of 1–42 kHz (6 kHz steps) with an SPL of 80 dB. Each stimulus entity was presented 300 times at 20 Hz and averaged. The red line indicates the onset of the acoustic stimulus (y-axis scaling has been adapted in (**C**)).

Identification of $W_{I\text{-}IV}$ was based on their latencies, i.e., W_I appeared 1.588 ± 0.025 ms and 1.527 ± 0.032 ms after the acoustic stimulus in females and males, respectively; W_{II} after 2.407 ± 0.045 ms in females and 2.389 ± 0.032 ms in males; W_{III} after 3.256 ± 0.056 ms in females and 3.197 ± 0.035 ms in males and W_{IV} after 4.419 ± 0.079 ms in females and 4.331 ± 0.049 ms in males at 65 dB SPL in $Ca_v3.2^{+/+}$ control animals (also see Fig. 12). The ABR amplitude growth function was analyzed for $W_{I\text{-}IV}$ (Fig. 11). Based on the nonexistence or rare appearance of deflections (waves) for low SPL (0–25 dB), wavelet analysis detected no, or only limited, confirmed accordance of waves. For higher SPL (40–90 dB), wavelet analysis detected almost all waves ($W_{I\text{-}IV}$) in experimental animals.

For W_I, regular two-way ANOVA revealed a significant interaction between GT and SPL, a significant effect of SPL and no significant GT effect on amplitude growth in either genders. Multiple comparisons identified a significant delay in amplitude increase with higher SPL values (40–75 dB) for both female and male $Ca_v3.2^{-/-}$ compared to $Ca_v3.2^{+/+}$ and $Ca_v3.2^{+/-}$ mice (Fig. 11A, B). With higher SPL levels (75–90 dB), W_I amplitude in $Ca_v3.2$ null mutant mice reached similar amplitude levels as observed in $Ca_v3.2^{+/+}$ and $Ca_v3.2^{+/-}$ mice. SPL-dependent increase in W_I amplitude is delayed in $Ca_v3.2^{-/-}$ mice, reaching control levels at high SPL >80 dB. These findings could be related to the predominant expression of $Ca_v3.2$ in IHCs, OHCs and the SGN.

W_{II} analysis revealed significance for an interaction between GT and SPL and an SPL effect, but no significant GT effect was observed in amplitude growth for female or male mice.

$Ca_v3.2^{-/-}$ female and male mice displayed significant delays in amplitude growth, revealed by Tukey´s multiple comparisons test within the SPL range of 40–60 dB (Fig. 11C, D). As amplitude levels of $Ca_v3.2^{+/+}$ and $Ca_v3.2^{+/-}$ in female and male mice

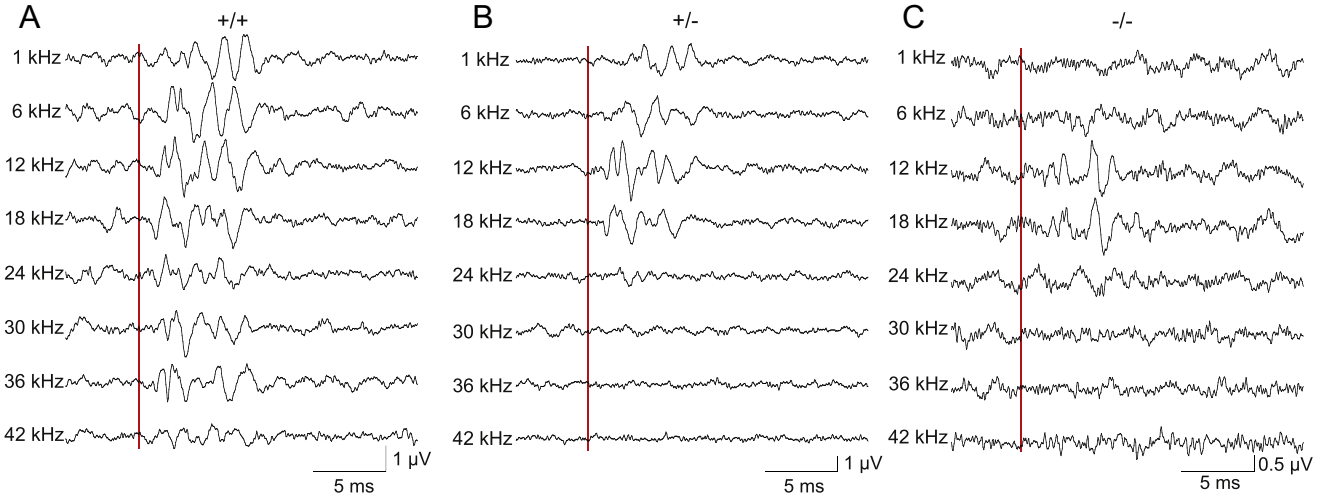

Fig. 7. Tone burst evoked ABRs in male $Ca_v3.2$ transgenic mice. Representative ABRs from $Ca_v3.2^{+/+}$ (**A**), $Ca_v3.2^{+/-}$ (**B**) and $Ca_v3.2^{-/-}$ (**C**) male mice (aged 140.67 ± 0.38 days) following tone bursts of 1–42 kHz (6 kHz steps) with an SPL of 80 dB. Each stimulus entity was presented 300 times at 20 Hz and averaged. The red line indicates the onset of the acoustic stimulus. Note that y-axis scaling has been adapted in (**C**).

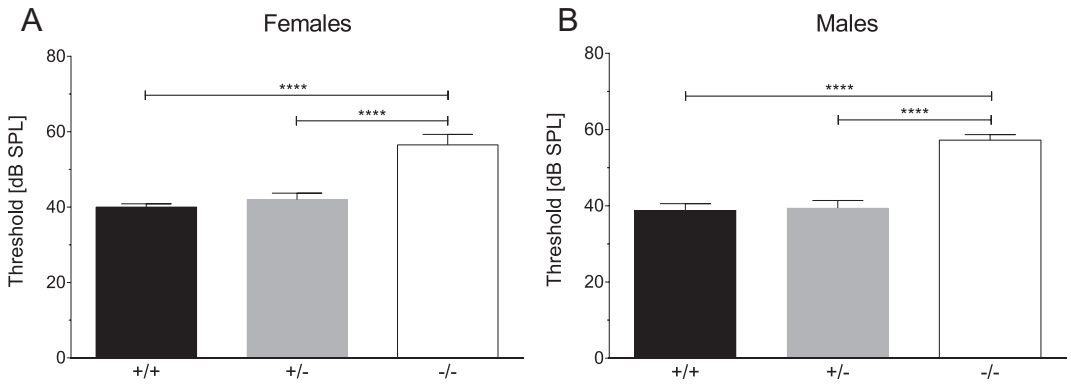

Fig. 8. Increased click-evoked ABR hearing thresholds in female and male $Ca_v3.2^{-/-}$ animals aged 20 wk. Click evoked audiometric hearing threshold of female **(A)** and male **(B)** $Ca_v3.2^{+/+}$ (♀, n = 12; ♂, n = 13), $Ca_v3.2^{+/-}$ (♀, n = 10; ♂, n = 9) and $Ca_v3.2^{-/-}$ (♀, n = 10; ♂, n = 9) mice aged 140.67 ± 0.38 days. One-way ANOVA followed by Tukey's multiple comparisons test revealed a significant difference in hearing thresholds between the genotypes (females, $F_{2, 29} = 23.10$, $P < .0001$; males, $F_{2, 28} = 33.23$, $P = < .0001$, ordinary one-way ANOVA). $Ca_v3.2^{-/-}$ mice exhibited significantly increased hearing thresholds compared to $Ca_v3.2^{+/+}$ controls: ♀, 56.5 ± 2.6 dB vs. 40.0 ± 0.9 dB, $P < .00001$; ♂, 57.2 ± 1.5 dB vs. 38.8 ± 1.8 dB, $P < .00001$. The same held true in comparison to $Ca_v3.2^{+/-}$ mice (♀, 56.5 ± 2.6 dB vs. 42.0 ± 1.7 dB, $P < .00001$; ♂, 57.2 ± 1.5 dB vs. 39.4 ± 1.9 dB, $P < .00001$. Data are plotted as the mean ± SEM.

dropped with higher SPL (80–90 dB), $Ca_v3.2^{-/-}$ amplitude levels of both genders became significantly higher. In $Ca_v3.2^{-/-}$ mice, reduced W_{II} amplitude indicates potential functional and/or structural impairment of the cochlear nucleus, which is in line with reports of robust cochlear $Ca_v3.2$ expression. With higher SPL, this effect is likely to be compensated, and amplitudes remain high.

For W_{III}, we confirmed a significant interaction between GT and SPL for $Ca_v3.2$ in male mice, no significant interaction in $Ca_v3.2$ female mice, a significant effect of SPL in both females and males, and no GT effect on amplitude growth. Tukey´s multiple comparisons test revealed no significant differences for $Ca_v3.2^{-/-}$ female mice compared to $Ca_v3.2^{+/-}$ and $Ca_v3.2^{+/+}$, but significantly higher amplitudes were observed for $Ca_v3.2^{+/-}$ female mice for SPL 85–90 dB compared to $Ca_v3.2^{+/+}$ (Fig. 11E, F). $Ca_v3.2^{-/-}$ males exhibited decreased amplitude at intermediate (55 dB) and higher (85–90 dB) SPL values. Although T-type VGCCs are supposed to be expressed in the SOC underlying W_{III}, only minor alterations in W_{III} amplitude were detected in $Ca_v3.2$ transgenic mice for both genders. Analysis of amplitude growth for W_{IV} revealed a significant interaction between GT and SPL in both genders, a significant GT effect for male mice, and a significant SPL effect in males and females. Both $Ca_v3.2^{-/-}$ female and male mice displayed significantly delayed amplitude growth and reduced W_{IV} amplitude levels compared to $Ca_v3.2^{+/+}$ and $Ca_v3.2^{+/-}$ mice (40–65 dB, Fig. 11G, H). Although no detailed information on $Ca_v3.2$ expression in the lateral leminiscus (LL) underlying W_{IV} is available, the delay observed in W_{IV} amplitude growth points to a functional role for $Ca_v3.2$ in LL auditory processing. Statistics were performed using two-way RM ANOVA and Tukey´s multiple comparisons test for all waves and genders.

Click-evoked ABR wave latency analysis

To investigate the role of $Ca_v3.2$ VGCCs on temporal auditory processing within the inner ear and brainstem, we analyzed absolute click evoked wave latencies by measuring

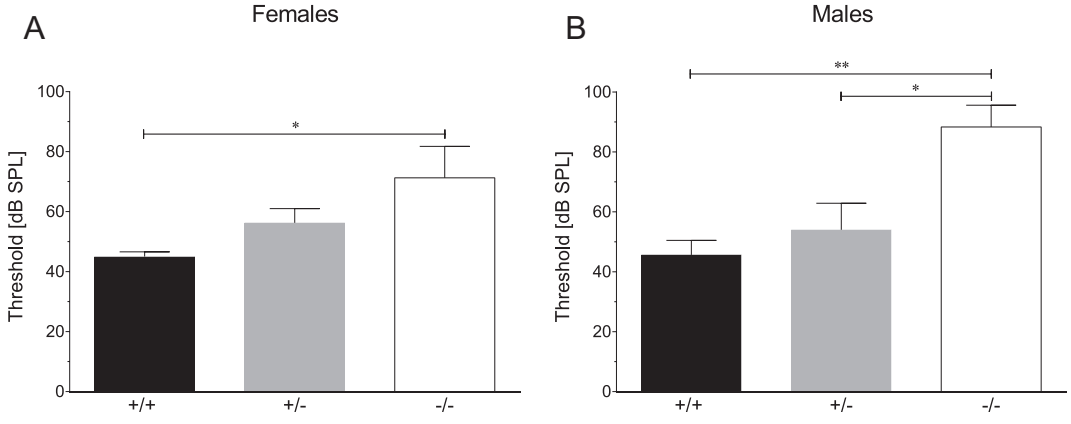

Fig. 9. Increased click-evoked ABR hearing thresholds in female and male $Ca_v3.2^{-/-}$ animals aged 40 wk. Click evoked hearing thresholds for female **(A)** and male **(B)** $Ca_v3.2^{+/+}$ (♀, n = 5; ♂, n = 8), $Ca_v3.2^{+/-}$ (♀, n = 4; ♂, n = 5) and $Ca_v3.2^{-/-}$ (♀, n = 4; ♂, n = 3) animals 280.72 ± 0.60 days old. One-Way ANOVA followed by Tukey's multiple comparisons test confirmed significantly increased hearing thresholds for $Ca_v3.2^{-/-}$ mice compared to controls in both genders: ♀, 71.3 ± 10.5 dB vs. 45.0 ± 1.6 dB, $P < .05$; ♂, 88.3 ± 4.2 dB vs. 45.6 ± 4.6 dB, $P < .01$. In males, the hearing threshold of α1H null mutants also exceeded the threshold of $Ca_v3.2^{+/-}$ mice: 88.3 ± 4.2 dB vs. 54.0 ± 6.6 dB, $P < .05$. Data are plotted as the mean ± SEM. Note that there is an overall increase in hearing threshold compared to study groups aged 140.67 ± 0.38 days.

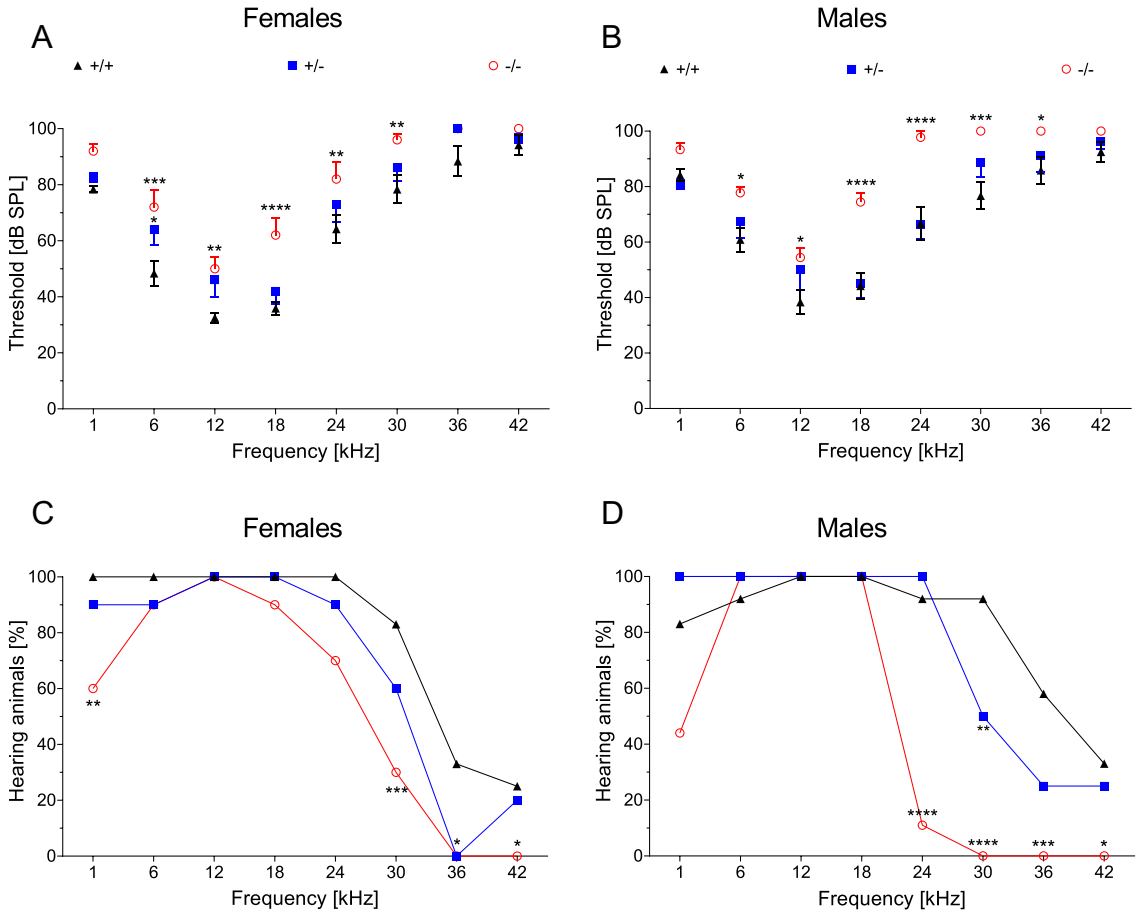

Fig. 10. Increased tone burst evoked ABR hearing thresholds in female and male $Ca_v3.2^{-/-}$ mice **(A, B)**. Tone burst (1–42 kHz, 6 kHz steps) evoked ABR based audiometric hearing thresholds for $Ca_v3.2^{+/+}$ (♀, n = 12; ♂, n = 12, ▲), $Ca_v3.2^{+/-}$ (♀, n = 10; ♂, n = 8, ■) and $Ca_v3.2^{-/-}$ animals (♀, n = 10; ♂, n = 9, ○) aged 140.67 ± 0.38 days. Significant interaction was observed for males regarding GT and stimulus frequency ($F_{14, 182}$ = 2.67, P = .0014), whereas no significant interaction was confirmed in female mice ($F_{14, 203}$ = 1,289; P = .216). Two-way RM ANOVA revealed significant effects of the genotype (♀, $F_{(2, 29)}$ = 11.20, P = .0002; ♂, $F_{(2, 26)}$ = 14.48, P < .0001), as well as the tested frequency, on the hearing threshold (♀, $F_{(7, 203)}$ = 107.4; ♂, $F_{(7, 182)}$ = 71.85; both P < .0001) for $Ca_v3.2^{-/-}$ females **(A)** and males **(B)**. Tukey's multiple comparisons test revealed significantly increased hearing thresholds for different stimulus frequencies in female **(A)** and male **(B)** $Ca_v3.2^{-/-}$ mice. **(C, D)** Percentage of animals with a detected hearing threshold for each frequency, illustrating significant genotype effects (**C**; ♀, $F_{(2, 29)}$ = 7.692, P = .0021; ♂, $F_{(2, 26)}$ = 19.16, P = .0001) and frequency effects (♀, $F_{(7, 203)}$ = 51.62, P < .0001; ♂, $F_{(7, 182)}$ = 41.92, P < .0001) on hearing ability. Unpaired two-way ANOVA also revealed a significant interaction between GT and frequency for male mice ($F_{14, 182}$ = 6.81, P < .0001), but no significant interaction for female mice ($F_{14, 203}$ = 1.360; P = .175). Tukey´s multiple comparisons test further demonstrated significant hearing loss in the higher frequency range (♀, > 30 kHz; ♂, > 24 kHz) for $Ca_v3.2^{-/-}$ females **(C)** and males **(D)** compared to $Ca_v3.2^{+/-}$ and $Ca_v3.2^{+/+}$ mice. Data are plotted as the mean ± SEM.

the processing time of each ABR wave (W_I–W_{IV}). First, this analysis was performed again at 65 dB SPL because resultant ABRs exhibited best fit using the automated complex "Mexican hat" based wavelet approach.

Statistical analysis revealed that W_I latency was increased in female $Ca_v3.2^{-/-}$ mice compared to controls (Fig. 12A). In males, W_I latency was increased in $Ca_v3.2^{-/-}$ mice compared to controls and $Ca_v3.2^{+/-}$ mice (Fig. 12B).

For W_{II}, female $Ca_v3.2^{+/-}$ and $Ca_v3.2^{-/-}$ mice displayed significantly increased latency compared to controls (Fig. 12C). In males, $Ca_v3.2^{-/-}$ mice exhibited significantly increased latency compared to controls and $Ca_v3.2^{+/-}$ mice (Fig. 12D).

No differences were observed in males for W_{III} latency (Fig. 12F). In females, only $Ca_v3.2^{+/-}$ displayed increased W_{III} latency compared to controls, but no difference was detected for $Ca_v3.2^{-/-}$ mice (Fig. 12E).

Finally, W_{IV} latency analysis revealed an increase in female $Ca_v3.2^{+/-}$ mice compared to controls (Fig. 12G) and an increase in male $Ca_v3.2^{-/-}$ mice compared to controls and $Ca_v3.2^{+/-}$ mice (Fig. 12H). Interestingly, gender specific differences were observed in heterozygous mice with female $Ca_v3.2^{+/-}$ mice exhibiting significantly higher latencies for W_I, W_{II}, W_{III} and W_{IV} than male $Ca_v3.2^{+/-}$ animals (P < 0.01). The reasons for these differences remain to be determined.

Finally, interwave-interval (IWI) analysis (i.e., interpeak latency (IPL) analysis) revealed a significant increase in $W_{I\text{-}IV}$ latency in female $Ca_v3.2^{+/-}$ mice compared to controls but not in female $Ca_v3.2^{-/-}$ mice (Fig. 13A). No alterations in IWI $\Delta W_{I,IV}$ were observed in male transgenic animals (Fig. 13B). Moreover, gender specific IWI differences were observed for $\Delta W_{I,IV}$ in $Ca_v3.2^{+/-}$ mice.

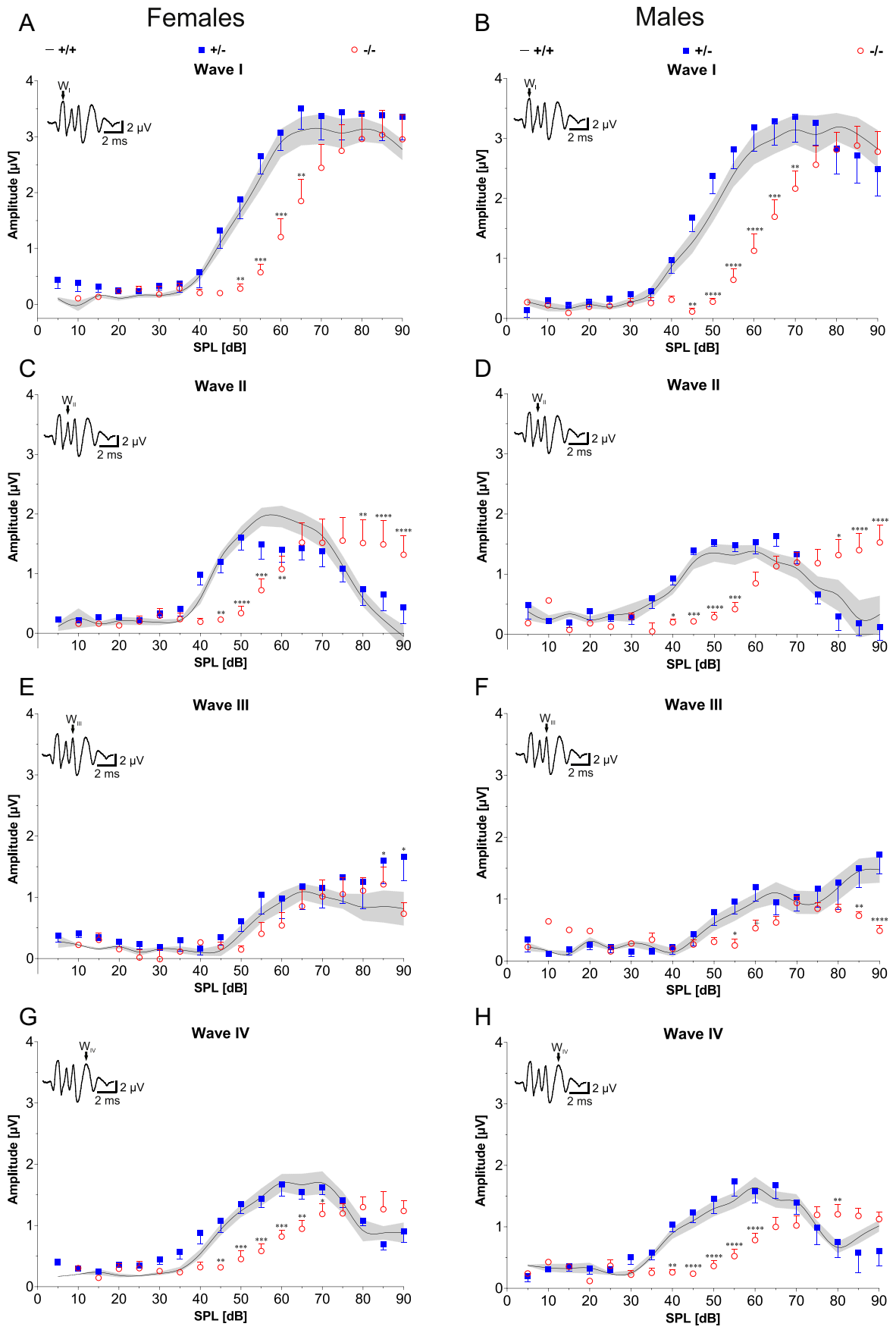
A
Females
B
Males
+/+
+/-
-/-
Wave I
Wave II
Wave III
Wave IV
2 µV
2 ms
Amplitude [µV]
SPL [dB]
C
D
E
F
G
H

In a second approach, latency analysis was performed at comparable sensation levels (20 dB above individual hearing thresholds). Under these conditions, no changes were observed in males from any of the three genotypes. In females, significant changes in W_{II}, W_{III} and W_{IV} latencies between controls and $Ca_v3.2^{+/-}$ mice persisted. We also observed a reduction in W_I latency in $Ca_v3.2^{-/-}$ mice compared to $Ca_v3.2^{+/-}$ mice (not shown).

Cochlear VGCC transcript levels in $Ca_v3.2$ transgenic mice

Various VGCCs are expressed in the murine cochlea, including HVA L-type $Ca_v1.2$ and $Ca_v1.3$ channels, HVA Non-L-type $Ca_v2.3$ channels and LVA T-type $Ca_v3.1$–$Ca_v3.3$ channels. qPCR was performed to assess for potential compensatory changes in transcript levels for these VGCCs. A gender specific analysis in $Ca_v3.2^{+/-}$ and $Ca_v3.2^{-/-}$ mice revealed that the above mentioned VGCCs exhibited no transcriptional changes that could account for the observed differences in click and tone burst related hearing thresholds, $W_{I\text{-}IV}$ amplitude growth function or $W_{I\text{-}IV}$ latencies (Figs. 14, 15, Table 2). In females, a statistical trend (P = .083) was detected for $Ca_v3.1$ transcripts in $Ca_v3.2^{-/-}$ compared to controls (Fig. 14D). In males, a statistical trend (P = .083) was observed for $Ca_v2.3$ transcripts in $Ca_v3.2^{-/-}$ mice compared to controls (Fig. 15C). Finally, a statistical trend (P = .065) was also observed for $Ca_v2.3$ transcripts between $Ca_v3.2^{-/-}$ males and females.

DISCUSSION

The pathophysiological implications of $Ca_v3.2$ VGCCs were previously reported to include alteration of mechanoreception (Wang and Lewin, 2011) and pain response (Choi et al., 2007; Tsubota et al., 2018), age-induced endothelial dysfunction (Thuesen et al., 2018), epilepsy (Becker et al., 2008; Zamponi et al., 2010), retinal dysfunction (Hamby et al., 2015), (sensory) neuronal hyperexcitability (Jacus et al., 2012; Voisin et al., 2016; Zhang et al., 2018), elevated anxiety, impaired memory and reduced sensitivity to psychostimulants (Gangarossa et al., 2014). In the auditory trace fear conditioning task, $Ca_v3.2^{-/-}$ mice performed normally but were impaired in context-cued trace fear conditioning (Chen et al., 2012). In addition, our longitudinal body weight analysis (Fig. 3B, C) indicates a complex developmental impairment, particularly in $Ca_v3.2^{-/-}$ mice, which could be related to the cardiovascular phenotype, consisting of constitutively constricted coronary arterioles and focal myocardial fibrosis in $Ca_v3.2$ deficient animals (Chen et al., 2003; Mizuta et al., 2010). Of note, established cardiovascular disease and individual or combined cardiovascular disease risk factors are associated with hearing loss (Erkan et al., 2015; Tan et al., 2018), although there are also studies that do not support this view (Haremza et al., 2017).

In our study, we performed gender specific analysis of both $Ca_v3.2^{+/-}$ mice, which do not display a cardiac phenotype, and $Ca_v3.2^{-/-}$ null mutant mice. Notably, the transgenic animals used in this study are from a C57Bl/6 background, which is important as their cochlea mimics typical characteristics of the aging human inner ear and can thus serve as a model of ARHL (presbycusis) (Ohlemiller, 2006). Age-related increases in ABR thresholds in the C57BL/6 strain become exacerbated approximately 8–9 months of age, predominately above 12 kHz (Spongr et al., 1997; Ison et al., 2007). As experimental animals were only 5 months of age in this study, our results represent the physiological implications of $Ca_v3.2$ in hearing physiology rather than its implications in hearing loss. Our study demonstrates that audiometric click ABR thresholds are increased in $Ca_v3.2^{-/-}$ mice from both genders compared to controls and $Ca_v3.2^{+/-}$ mice at 20 wk and 40 wk of age (Figs. 8, 9). No significant changes were observed for heterozygous mice compared to controls. Similar results were observed for tone burst derived ABR thresholds in both genders at the age of 20 wk (Fig. 10A, B). Lei et al. (2011) previously reported that they did not detect any significant ABR threshold shifts in $Ca_v3.2^{-/-}$ mice from 9–11 months of age compared to controls, suggesting a preserving effect of $Ca_v3.2$ ablation on age-related increases in ABR thresholds. This is in contrast to the increased click and tone burst related ABR thresholds in $Ca_v3.2^{-/-}$ mice, which we observe at an earlier developmental stage (20 wk) in both genders.

Of note, Ca_v3 VGCCs exhibit a complex developmental expression pattern within the cochlea (Lei et al., 2011; Yu et al., 2015, 2016). Although previous studies indicated that T-type Ca^{2+} channels can also be detected in various other

Fig. 11. Click-evoked ABR amplitude growth function analysis of Wave I–IV in female (left) and male (right) $Ca_v3.2$ transgenic mice and controls.Wave I–IV amplitude (μV) plotted as a function of increasing SPL (dB) for click-evoked ABR wave analysis in $Ca_v3.2^{+/+}$ (♀, n = 12; ♂, n = 11; black line represents the approximate control curve, including the 95% confidence interval in grey), $Ca_v3.2^{+/-}$ (♀, n = 8; ♂, n = 7, ■) and $Ca_v3.2^{-/-}$ animals (♀, n = 7; ♂, n = 9, ○) aged 140.67 ± 0.38 days. Both $Ca_v3.2^{-/-}$ female and male mice exhibit significantly delayed increases in amplitude growth across increasing SPL for wave I **(A, B)**, wave II **(C, D)**, and wave IV **(G, H)** compared to $Ca_v3.2^{+/+}$ and $Ca_v3.2^{+/-}$ mice. **(E, F)** For wave III, only $Ca_v3.2^{-/-}$ male mice displayed significantly delayed amplitude growth across increasing SPL compared to female $Ca_v3.2^{-/-}$ animals.For W_I, regular two-way ANOVA also revealed a significant interaction in GT and SPL (female: $F_{20, 240}$ = 4.924, P < .0001; male $F_{22, 264}$ = 8.767, P < .0001), a significant effect of SPL (female: $F_{10, 240}$ = 108.6, P < .0001; male: $F_{11, 264}$ = 112.3, P < .0001) and no significant GT effect on amplitude growth. W_{II} analysis displayed significance for GT and SPL interaction (female: $F_{22, 253}$ = 9.629, P < .0001; male: $F_{22, 264}$ = 11.01, P < .0001), SPL effect (female: $F_{11, 253}$ = 21.50, P < .0001; male: $F_{11, 264}$ = 10.67, P < .0001) but no significant GT effect on amplitude growth for either female or male mice. For W_{III}, we confirmed a significant GT and SPL interaction for $Ca_v3.2$ male mice ($F_{22, 264}$ = 3.656, P < .0001), no significant interaction for $Ca_v3.2$ female mice, a significant effect of SPL (female: $F_{11, 253}$ = 17.91, P < .0001; male: $F_{11, 264}$ = 33.25, P < .0001) and no GT effect on amplitude growth. Finally, analysis of amplitude growth for W_{IV} showed a significant interaction between GT and SPL (female: $F_{22, 264}$ = 6.699, P < .0001; male: $F_{22, 264}$ = 11.05, P < .0001), a significant GT effect for male mice ($F_{2, 24}$ = 3.937, P = .0332), and a significant SPL effect (female: $F_{11, 264}$ = 29.67, P < .0001; male $F_{11, 264}$ = 20.17, P < .0001). Data are presented as the mean ± SEM.

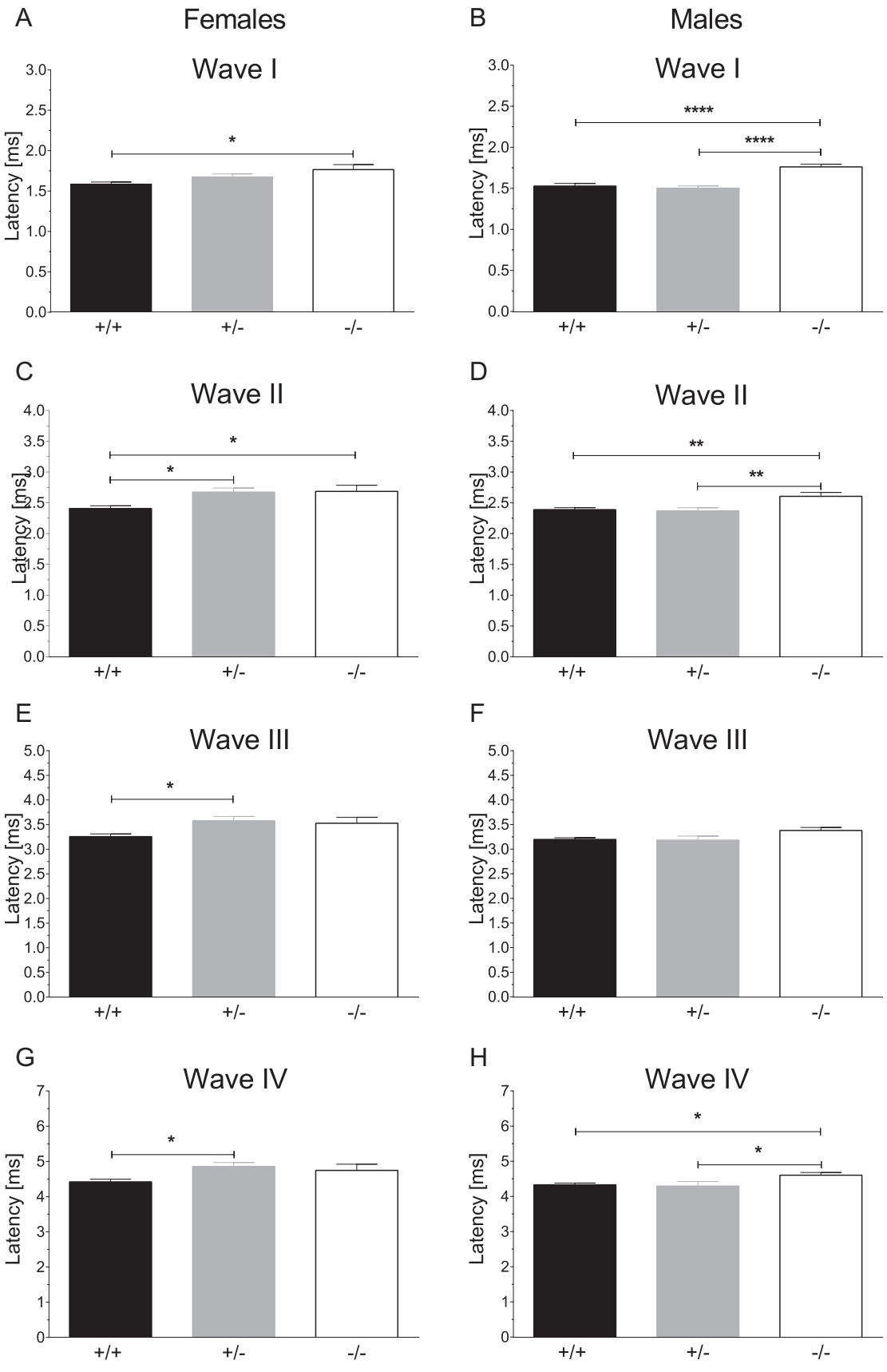
A
Females
Wave I
B
Males
Wave I
C
Wave II
D
Wave II
E
Wave III
F
Wave III
G
Wave IV
H
Wave IV
Latency [ms]
+/+
+/-
-/-
*
**
****

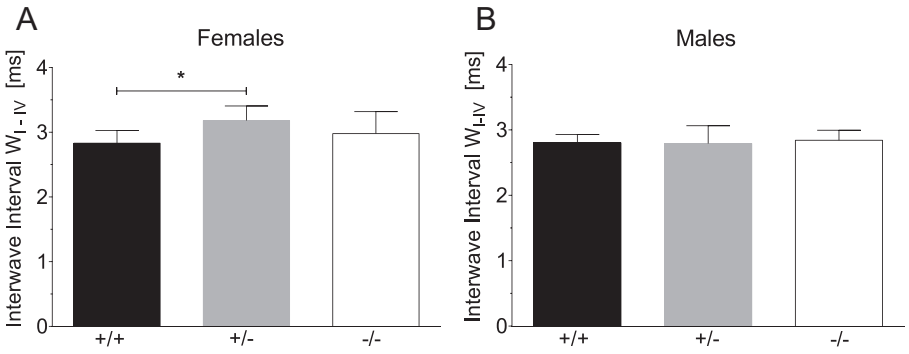

Fig. 13. Interwave-interval (IWI) analysis. Female (**A**) and male (**B**) $Ca_v3.2^{+/+}$ (♀, n = 12; ♂, n = 11), $Ca_v3.2^{+/-}$ (♀, n = 8; ♂, n = 7) and $Ca_v3.2^{-/-}$ mice (♀, n = 8; ♂, n = 9) were evaluated for alterations in IWI. Despite complex changes in absolute latencies, IWI alterations were only observed in $\Delta W_{I,IV}$ for female $Ca_v3.2^{+/-}$ mice compared to controls (3.182 ± 0.079 ms (n = 8) vs. 2.831 ± 0.057 ms (n = 12), $P < .05$) but not in female $Ca_v3.2^{-/-}$ mice (2.979 ± 0.120 ms (n = 8). No changes were detected for IWI $\Delta W_{I,IV}$ in males. Gender specific IWI differences were observed for $\Delta W_{I,IV}$ in $Ca_v3.2^{+/-}$ mice (3.182 ± 0.079 ms (♀, n = 8) vs. 2.792 ± 0.103 ms (♂, n = 7), $P < .01$). Data are depicted as the mean ± SEM.

structures of the auditory tract, detailed information about their spatiotemporal expression pattern is still lacking. In 2 month old C57Bl/6 mice, $Ca_v3.1$ and $Ca_v3.3$ VGCCs are only weakly expressed in the organ of Corti, i.e., $Ca_v3.1$ in OHCs, IHCs, pillar cells, Deiters cells, and OHCs and $Ca_v3.3$ in OHCs and Deiters cells. Interestingly, no immunoreaction was detected for $Ca_v3.2$ (Shen et al., 2007). In contrast, $Ca_v3.2$ expression was dominant in the SGNs, while only moderate levels of $Ca_v3.1$ and $Ca_v3.3$ were observed in this region (Shen et al., 2007). Real-time PCR revealed murine cochlear $Ca_v3.2$ transcript levels that exceeded those of $Ca_v3.1$ and $Ca_v3.3$ by 2-fold and 100-fold, respectively. Quantification of T-type Ca^{2+} channels in the cochlea of 6–8 wk old C57BL/6J mice revealed transcripts of all three T-type channels with $Ca_v3.2$ displaying the lowest expression (Yu et al., 2016). Lei et al. (2011) analyzed all three LVA Ca_v3 transcript levels in the organ of Corti at 2, 4 and 8 months of age in which $Ca_v3.2$ T-type channels clearly predominate and increase with age (Lei et al., 2011). This tendency was also confirmed in the SGN from mice 6–44 wk old in which $Ca_v3.2$ transcripts represent the major T-type component (Yu et al., 2015).

Overall, $Ca_v3.2$ VGCCs exhibit complex species specific spatiotemporal expression patterns in the auditory tract, particularly within the cochlea. Clearly, $Ca_v3.2$ expression continuously increases with age, and particularly at later stages (9–11 months), $Ca_v3.2$ exerts devastating effects on SGN viability, which manifests upon $Ca_v3.2$ ablation (Lei et al., 2011). However, at earlier developmental stages, e.g., 20 wk of age, our data suggest an alternative, i.e., physiological role, of $Ca_v3.2$ VGCCs that is distinct from its pathophysiological implications in ARHL. Indeed, the complex alterations in hearing thresholds (Figs. 8, 10), W_{I-IV} amplitude growth function (Fig. 11) and W_{I-IV} latencies (Fig. 12) in $Ca_v3.2^{+/-}$ and $Ca_v3.2^{-/-}$ mice suggest important functional implications in the HCs / SGN, NC, SOC and the LL, indicating that $Ca_v3.2$ is a prerequisite for precise auditory information processing in young adult C57Bl/6 mice. Of note, latency analysis under comparable sensation levels revealed minor changes that may indicate a more prominent role of $Ca_v3.2$ VGCCs within the cochlea. In addition, it has to be considered that C57BL/6 mice, in contrast to CBA animals, display cadherin 23 related ARHL (Johnson et al., 2017). Thus, we cannot exclude that the genetic modification of $Ca_v3.2$ in our mouse lines potentially interferes with cadherin 23 mutation in these animals, potentially influencing observed results (Kane et al., 2012; Johnson et al., 2017).

Little information is currently available regarding expression of $Ca_v3.2$ in the ascending auditory tract, which creates challenges in attributing specific wave amplitude and wave latency alterations to specific electrophysiological alterations at the cellular level. LVA Ca^{2+} channels have been identified in Cartwheel cells of the dorsal cochlear nucleus. Cartwheel cells can fire both simple and complex action potential patterns, and early complex spike firing patterns and afterdepolarisations in these cells requires T-type and R-type Ca^{2+} channels but also BK and SK channels (Kim and Trussell, 2007). In the LSO, the firing rate of principal neurons is a linear function of interaural sound intensity differences. This type of linear response has been hypothesized to result from integration of excitatory

Fig. 12. Click-evoked ABR based wave I–IV latency analysis of female (left) and male (right) $Ca_v3.2$ transgenic mice and controls. Latencies (ms) for each ABR wave (I–IV) at 65 dB SPL are depicted for $Ca_v3.2^{+/+}$ (♀, n = 12; ♂, n = 11), $Ca_v3.2^{+/-}$ (♀, n = 8; ♂, n = 7) and $Ca_v3.2^{-/-}$ (♀, n = 8; ♂, n = 9) female (**A, C, E, G**) and male (**B, D, F, H**) mice aged 140.67 ± 0.38 days. Tukey's multiple comparisons test revealed that W_I latency was increased in female $Ca_v3.2^{-/-}$ mice compared to controls (1.766 ± 0.062 ms (n = 8) vs. 1.588 ± 0.025 ms (n = 12), $P < .05$, A). In males, W_I latency was increased in $Ca_v3.2^{-/-}$ mice (1.762 ± 0.031 ms, n = 9) compared to controls (1.527 ± 0.032 ms, n = 11, $P < .0001$) and $Ca_v3.2^{+/-}$ mice (1.502 ± 0.028 ms, n = 7, $P < .0001$, B). For W_{II}, female $Ca_v3.2^{+/-}$ and $Ca_v3.2^{-/-}$ mice displayed significantly increased latency compared to controls (2.673 ± 0.066 ms (n = 8) vs. 2.407 ± 0.045 ms (n = 12), $P < .05$; 2.685 ± 0.099 ms (n = 8) vs. 2.407 ± 0.045 ms (n = 12), $P < .05$, **C**). In males, $Ca_v3.2^{-/-}$ mice exhibited significantly increased latency compared to controls (2.606 ± 0.063 ms (n = 9) vs. 2.389 ± 0.032 ms (n = 11), $P < .01$) and $Ca_v3.2^{+/-}$ mice (2.606 ± 0.063 ms (n = 9) vs. 2.369 ± 0.051 ms (n = 7), $P < .01$, **D**). No differences were observed in males for W_{III} latency ($Ca_v3.2^{+/+}$, 3.197 ± 0.035 ms (n = 11); $Ca_v3.2^{+/-}$, 3.182 ± 0.083 ms (n = 7); $Ca_v3.2^{-/-}$, 3.379 ± 0.061 ms (n = 9), **F**). In females, only $Ca_v3.2^{+/-}$ displayed increased W_{III} latency compared to controls (3.578 ± 0.087 ms (n = 8) vs. 3.256 ± 0.056 ms (n = 12), $P < .05$), but no difference was detected for $Ca_v3.2^{-/-}$ (3.529 ± 0.121 ms (n = 8) vs. 3.256 ± 0.056 ms (n = 12), **E**). W_{IV} latency analysis revealed an increase in female $Ca_v3.2^{+/-}$ mice compared to controls (4.857 ± 0.111 ms (n = 8) vs. 4.419 ± 0.079 ms (n = 12), $P < .05$, **G**) and an increase in male $Ca_v3.2^{-/-}$ mice compared to controls (4.603 ± 0.077 ms (n = 9) vs. 4.331 ± 0.049 ms (n = 11), $P < .05$) and $Ca_v3.2^{+/-}$ mice (4.603 ± 0.077 ms (n = 9) vs. 4.294 ± 0.130 ms (n = 7), $P < .05$, **H**). One-way ANOVA revealed a significant difference in latency for all four waves between all three genotypes in both female and male animals. Data are depicted as the mean ± SEM.

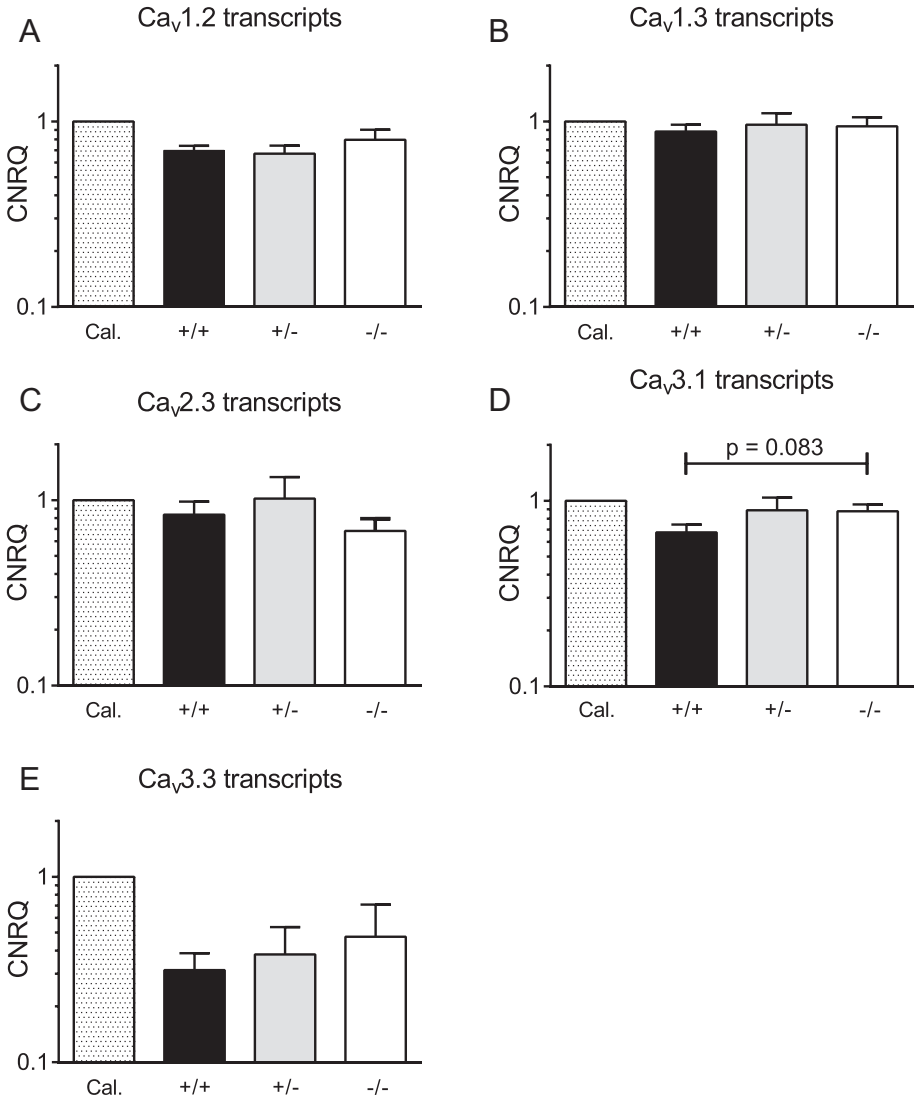

Fig. 14. Cochlear VGCC transcripts in female $Ca_v3.2$ transgenic mice. RNA was isolated from the cochlea of female $Ca_v3.2^{+/+}$ (n = 8), $Ca_v3.2^{+/-}$ (n = 8) and $Ca_v3.2^{-/-}$ (n = 8) mice for real-time PCR (qPCR) to assess for alterations in other VGCC ($Ca_v1.2$, $Ca_v1.3$, $Ca_v2.3$, $Ca_v3.1$ and Ca_v 3.3) transcript levels. No significant changes were observed for the VGCCs tested. A statistical trend was detected for $Ca_v3.1$ transcripts. CNRQ, Calibrated Normalized Relative Quantity; Cal, Calibrator.

ipsilateral and inhibitory contralateral inputs. A previous study (Adam et al., 2001) demonstrated that this complex spike activity in rat LSO was based on T-type Ca^{2+} currents, subthreshold Na^+ currents and hyperpolarization-activated I_h conductance being sensitive to Ni^{2+}, tetrodotoxin (TTX) and Cs^+, respectively (Adam et al., 2001). Of note, $Ca_v1.3$ VGCCs, which are known to be relevant for auditory function in IHCs, share basic electrophysiological properties similar to those of LVA channels, such as rapid activation kinetics (Koschak et al., 2001; Xu and Lipscombe, 2001; Zampini et al., 2010; Inagaki and Lee, 2013; Zampini et al., 2013). The latter are important for temporal aspects of sound coding and the ability to accurately trigger firing of the auditory nerve to reflect sound frequency (phase locking). Also, $Ca_v1.3$ channels activate at relatively negative potentials (~-70 mV in immature IHCs) which is a major property of LVA channels as well (Koschak et al., 2001; Xu and Lipscombe, 2001; Zampini et al., 2010). Thus, given a RMP of ~-60 mV in these cells (Marcotti et al., 2003), both $Ca_v1.3$ and $Ca_v3.2$ may support tonic transmitter release at rest and effectively couple increased sound intensities with higher rates of transmitter release. Mechanistically, $Ca_v3.2$ might contribute to these processes by involvement in the complex spatiotemporal interdependence of intracellular Ca^{2+} levels and Ca^{2+} activated K^+ currents (particularly via BK) in HCs as has been previously shown for $Ca_v1.3$ as well (Joiner and Lee, 2015).

Despite these physiological implications, Ca^{2+} influx and Ca^{2+} signaling have been correlated with age-related and noise-induced neuronal cell death in HCs and SGN for some time. Consequently, T-type Ca^{2+} channel blockers were thought to be otoprotective in the setting of acquired hearing loss. Early studies suggested that trimethadione, ethosuximide and flunarizine were effective in protecting SGN and NIHL (So et al., 2005; Shen et al., 2007; Lei et al., 2011). Bao et al. (2013) confirmed this beneficial effect in NIHL for ethosuximide (Gomora et al., 2001) and zonisamide (Matar et al., 2009) for cochlear HCs and SGN. Accordingly, beneficial effects of T-type blockers on ABR threshold and SGN were also confirmed for ARHL using trimethadione, ethosuximide (Lei et al., 2011) and zonisamide (Yu et al., 2015). Importantly, the pharmaceutical drugs investigated have a multi-target character and do not exhibit selective T-type Ca^{2+} channel blocker characteristics. In contrast, in the aforementioned studies using 9–11 month old mice, T-type blockers preserved ABR thresholds and prevented excessive HC and SGN loss, Yu et al. (2016) reported the inverse in younger mice aged 24–26 wk. In a tone burst ABR setup, administration of mibefradil and benidipine did not have any beneficial impact on hearing thresholds at 8 Hz, 16 Hz and 32 kHz (despite at 24 kHz). Importantly, morphological changes were detected in IHCs and OHCs exhibiting disorganized and sparse stereocilia upon mibefradil administration and cell loss upon benidipine administration, respectively (Yu et al., 2016).

Together with our findings, these observations clearly indicate that $Ca_v3.2$ VGCCs exert profound physiological effects in young adults that are tremendously important for

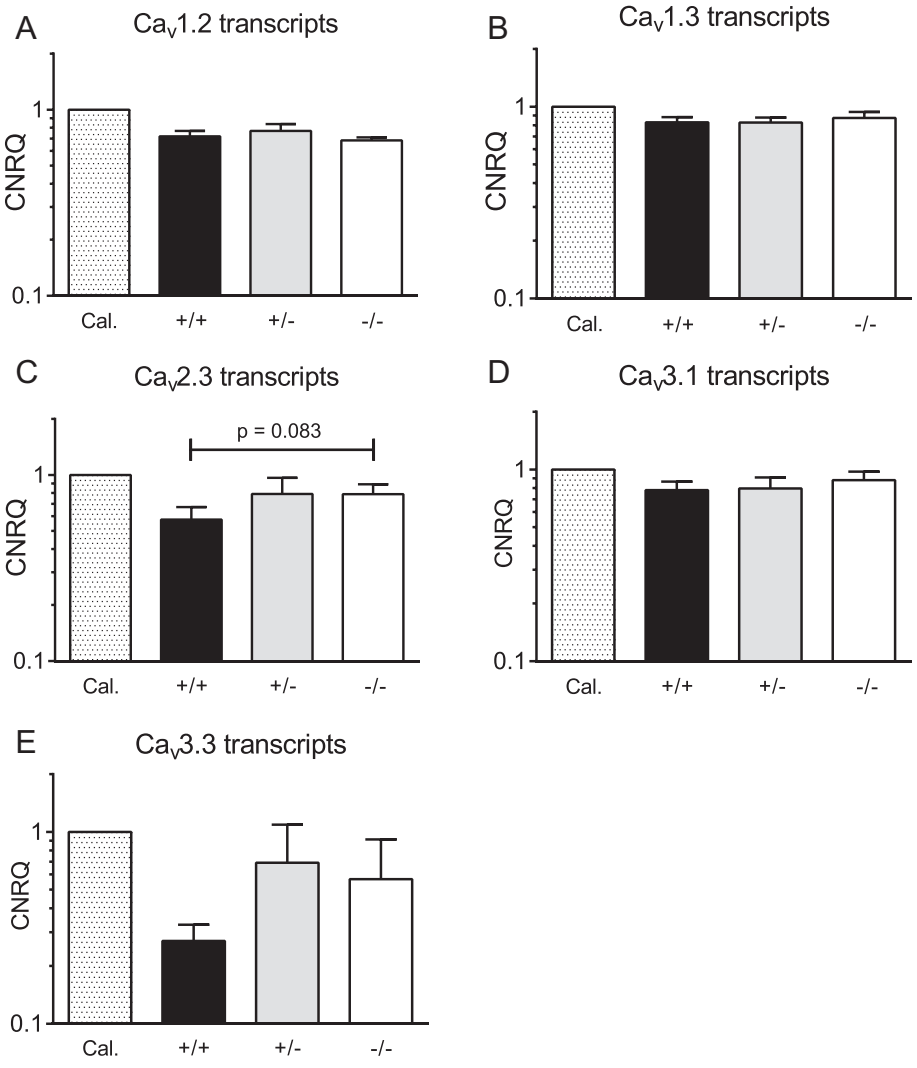

Fig. 15. Cochlear VGCC transcripts in male $Ca_v3.2$ transgenic mice. RNA was isolated from the cochlea of male $Ca_v3.2^{+/+}$ (n = 8), $Ca_v3.2^{+/-}$ (n = 8) and $Ca_v3.2^{-/-}$ (n = 8) mice for real-time PCR (qPCR) to assess for alterations in other VGCC ($Ca_v1.2$, $Ca_v1.3$, $Ca_v2.3$, $Ca_v3.1$ and $Ca_v3.3$) transcript levels. No significant changes were observed for the VGCCs tested. A statistical trend was detected for $Ca_v2.3$ transcripts. CNRQ, Calibrated Normalized Relative Quantity; Cal, Calibrator.

regular auditory processing within the ascending auditory pathway. However, within settings of acquired sensorineural hearing loss related to age or noise, increased $Ca_v3.2$ expression levels are likely to exert devastating effects on HC and SGN viability. Thus, we propose two pharmacotherapeutic constellations that need to be clearly differentiated: 1. late-stage treatment of ARHL and acoustic injury related NIHL in which animals/patients benefit from T-type blocker administration, and 2. early -stage application of T-type antagonists primarily related to epilepsy treatment in infants, children and young adults. In the latter group, application of T-type blockers was reportedly exerts potential negative effects on hearing up to transient/permanent hearing loss (Hori et al., 2003; Yeap et al., 2014; Hamed, 2017) (see also EMA side effect database, FDA adverse events reporting system (FAERS)). This is in full agreement with our findings that $Ca_v3.2$ is mandatory for functional and developmental integrity in the auditory system in adult mice.

PERSPECTIVES

$Ca_v3.2$ T-type Ca^{2+} channels are expressed in HCs and SGNs and T-type blockers have recently been suggested as effective for the prevention and treatment of ARHL and NIHL. Our studies demonstrate that $Ca_v3.2$ Ca^{2+} channels mediate important physiological functions for proper auditory information processing in the cochlea and ascending auditory tract in young adult mice. This is in contrast to the suggested otoprotective function of T-type blockers during older age. Consequently, the young adult stage could represent a vulnerable phase in which T-type blockers might exert deleterious effects on the peripheral auditory system that impact potential pharmaceutical T-type blocker treatment of ARHL and NIHL.

ACKNOWLEDGMENTS

The authors would like to thank Dr. Christina Kolb (German Center for Neurodegenerative Diseases, DZNE) and Dr. Robert Stark (DZNE) for assistance in animal breeding and animal health care. This work was financially supported by the Federal Institute for Drugs and Medical Devices (Bundesinstitut für Arzneimittel und Medizinprodukte, BfArM, Bonn, Germany).

CONFLICT OF INTEREST

The authors declare that this research was performed in the absence of any commercial or financial relationships that could be construed as a potential conflict of interest.

Table 2. VGCC fold changes in cochleae from female (A) and male (B) controls (WT), $Ca_v3.2^{+/-}$ (HT) and $Ca_v3.2^{-/-}$ (KO) mice. Quantification results from 8 animals from each every genotype were normalized to a calibrator (positive control; cochleae from C57Bl6 animals) and fold changes (FC) were compared using Mann Whitney test in qBase plus software.

A)

	HT/WT		KO/WT		HT/KO	
VGCC Ca_v-α_1	*FC*	*P value*	*FC*	*P value*	*FC*	*P value*
$Ca_v1.3$	1.050	0.798	1.056	0.721	-1.006	0.878
$Ca_v1.2$	-1.064	0.382	1.087	0.798	-1.156	0.505
$Ca_v2.3$	1.076	0.959	-1.188	0.574	1.278	0.574
$Ca_v3.1$	1.264	0.505	1.323	0.083	-1.047	0.574
$Ca_v3.3$	1.095	0.798	1.040	0.878	1.053	0.959

B)

	HT/WT		KO/WT		HT/KO	
VGCC Ca_v-α_1	*FC*	*P value*	*FC*	*P value*	*FC*	*P value*
$Ca_v1.3$	-1.002	0.798	1.044	0.505	-1.046	0.798
$Ca_v1.2$	1.060	0.721	1.036	0.505	1.098	0.645
$Ca_v2.3$	1.290	0.442	1.417	0.083	-1.099	0.798
$Ca_v3.1$	-1.010	0.959	1.125	0.442	-1.136	0.505
$Ca_v3.3$	1.472	0.505	1.298	0.721	1.134	0.959

REFERENCES

Adam TJ, Finlayson PG, Schwarz DW. (2001) Membrane properties of principal neurons of the lateral superior olive. J Neurophysiol 86:922-934.

Alvarado JC, Fuentes-Santamaria V, Gabaldon-Ull MC, Blanco JL, Juiz JM. (2014) Wistar rats: a forgotten model of age-related hearing loss. Front Aging Neurosci 6:29.

Bao J, Lei D, Du Y, Ohlemiller KK, Beaudet AL, Role LW. (2005) Requirement of nicotinic acetylcholine receptor subunit beta2 in the maintenance of spiral ganglion neurons during aging. J Neurosci 25:3041-3045.

Bao J, Hungerford M, Luxmore R, Ding D, Qiu Z, Lei D, Yang A, Liang R, Ohlemiller KK. (2013) Prophylactic and therapeutic functions of drug combinations against noise-induced hearing loss. Hear Res 304:33-40.

Becker AJ, Pitsch J, Sochivko D, Opitz T, Staniek M, Chen CC, Campbell KP, Schoch S, Yaari Y, Beck H. (2008) Transcriptional upregulation of $Ca_v3.2$ mediates epileptogenesis in the pilocarpine model of epilepsy. J Neurosci 28:13341-13353.

Bogaerts S, Clements JD, Sullivan JM, Oleskevich S. (2009) Automated threshold detection for auditory brainstem responses: comparison with visual estimation in a stem cell transplantation study. BMC Neurosci 10:104.

Buchholz JN, Behringer EJ, Pottorf WJ, Pearce WJ, Vanterpool CK. (2007) Age-dependent changes in Ca^{2+} homeostasis in peripheral neurones: implications for changes in function. Aging Cell 6:285-296.

Chen CC, Lamping KG, Nuno DW, Barresi R, Prouty SJ, Lavoie JL, Cribbs LL, England SK, Sigmund CD, Weiss RM, Williamson RA, Hill JA, Campbell KP. (2003) Abnormal coronary function in mice deficient in alpha1H T-type Ca^{2+} channels. Science 302:1416-1418.

Chen CC, Shen JW, Chung NC, Min MY, Cheng SJ, Liu IY. (2012) Retrieval of context-associated memory is dependent on the $Ca_v3.2$ T-type calcium channel. PLoS One 7e29384.

Chen J, Chu H, Xiong H, Yu Y, Huang X, Zhou L, Chen Q, Bing D, Liu Y, Wang S, Cui Y. (2013) Downregulation of $Ca_v1.3$ calcium channel expression in the cochlea is associated with age-related hearing loss in C57BL/6J mice. Neuroreport 24:313-317.

Choi S, Na HS, Kim J, Lee J, Lee S, Kim D, Park J, Chen CC, Campbell KP, Shin HS. (2007) Attenuated pain responses in mice lacking $Ca_v3.2$ T-type channels. Genes Brain Behav 6:425-431.

Daubechies I. (1992) Ten lectures on wavelets. Philadelphia, PA: Society for Industrial and Applied Mathematics, 1992.

Du P, Kibbe WA, Lin SM. (2006) Improved peak detection in mass spectrum by incorporating continuous wavelet transform-based pattern matching. Bioinformatics 22:2059-2065.

Erkan AF, Beriat GK, Ekici B, Dogan C, Kocaturk S, Tore HF. (2015) Link between angiographic extent and severity of coronary artery disease and degree of sensorineural hearing loss. Herz 40:481-486.

Felix RA, Fridberger A, Leijon S, Berrebi AS, Magnusson AK. (2011) Sound rhythms are encoded by postinhibitory rebound spiking in the superior paraolivary nucleus. J Neurosci 31:12566-12578.

Gangarossa G, Laffray S, Bourinet E, Valjent E. (2014) T-type calcium channel $Ca_v3.2$ deficient mice show elevated anxiety, impaired memory and reduced sensitivity to psychostimulants. Front Behav Neurosci 8:92.

Gates GA, Mills JH. (2005) Presbycusis. Lancet 366:1111-1120.

Gates GA, Cobb JL, D'Agostino RB, Wolf PA. (1993) The relation of hearing in the elderly to the presence of cardiovascular disease and cardiovascular risk factors. Arch Otolaryngol Head Neck Surg 119:156-161.

Glueckert R, Wietzorrek G, Kammen-Jolly K, Scholtz A, Stephan K, Striessnig J, Schrott-Fischer A. (2003) Role of class D L-type Ca^{2+} channels for cochlear morphology. Hear Res 178:95-105.

Gomora JC, Daud AN, Weiergraber M, Perez-Reyes E. (2001) Block of cloned human T-type calcium channels by succinimide antiepileptic drugs. Mol Pharmacol 60:1121-1132.

Hamby AM, Rosa JM, Hsu CH, Feller MB. (2015) $Ca_v3.2$ KO mice have altered retinal waves but normal direction selectivity. Vis Neurosci 32:E003.

Hamed SA. (2017) The auditory and vestibular toxicities induced by antiepileptic drugs. Expert Opin Drug Saf 16:1281-1294.

Haremza C, Klopp-Dutote N, Strunski V, Page C. (2017) Evaluation of cardiovascular risks and recovery of idiopathic sudden sensorineural hearing loss in hospitalised patients: comparison between complete and partial sudden sensorineural hearing loss. J Laryngol Otol 131:919-924.

Hellemans J, Mortier G, De Paepe A, Speleman F, Vandesompele J. (2007) qBase relative quantification framework and software for management and automated analysis of real-time quantitative PCR data. Genome Biol 8:R19.

Henry KR. (2004) Males lose hearing earlier in mouse models of late-onset age-related hearing loss; females lose hearing earlier in mouse models of early-onset hearing loss. Hear Res 190:141-148.

Hirtz JJ, Boesen M, Braun N, Deitmer JW, Kramer F, Lohr C, Muller B, Nothwang HG, Striessnig J, Lohrke S, Friauf E. (2011) $Ca_v1.3$ calcium channels are required for normal development of the auditory brainstem. J Neurosci 31:8280-8294.

Hori A, Kataoka S, Sakai K, Hirose G, Iwasaki N, Horiguchi A, Takashima M, Tomoda K. (2003) Valproic acid-induced hearing loss and tinnitus. Intern Med 42:1153-1154.

Inagaki A, Lee A. (2013) Developmental alterations in the biophysical properties of $Ca_v1.3$ Ca^{2+} channels in mouse inner hair cells. Channels (Austin) 7:171-181.

Inagaki A, Ugawa S, Yamamura H, Murakami S, Shimada S. (2008) The $Ca_v3.1$ T-type Ca^{2+} channel contributes to voltage-dependent calcium currents in rat outer hair cells. Brain Res 1201:68-77.

Ison JR, Allen PD, O'Neill WE. (2007) Age-related hearing loss in C57BL/6J mice has both frequency-specific and non-frequency-specific components that produce a hyperacusis-like exaggeration of the acoustic startle reflex. J Assoc Res Otolaryngol 8:539-550.

Jacus MO, Uebele VN, Renger JJ, Todorovic SM. (2012) Presynaptic $Ca_v3.2$ channels regulate excitatory neurotransmission in nociceptive dorsal horn neurons. J Neurosci 32:9374-9382.

Johnson KR, Tian C, Gagnon LH, Jiang H, Ding D, Salvi R. (2017) Effects of Cdh23 single nucleotide substitutions on age-related hearing loss in C57BL/6 and 129S1/Sv mice and comparisons with congenic strains. Sci Rep 744450.

Joiner ML, Lee A. (2015) Voltage-Gated Ca_v1 Channels in Disorders of Vision and Hearing. Curr Mol Pharmacol 8:143-148.

Kane KL, Longo-Guess CM, Gagnon LH, Ding D, Salvi RJ, Johnson KR. (2012) Genetic background effects on age-related hearing loss associated with Cdh23 variants in mice. Hear Res 283:80-88.

Kim Y, Trussell LO. (2007) Ion channels generating complex spikes in cartwheel cells of the dorsal cochlear nucleus. J Neurophysiol 97:1705-1725.

Knipper M, Van Dijk P, Nunes I, Ruttiger L, Zimmermann U. (2013) Advances in the neurobiology of hearing disorders: recent developments regarding the basis of tinnitus and hyperacusis. Prog Neurobiol 111:17-33.

Koschak A, Reimer D, Huber I, Grabner M, Glossmann H, Engel J, Striessnig J. (2001) alpha 1D ($Ca_v1.3$) subunits can form l-type Ca^{2+} channels activating at negative voltages. J Biol Chem 276:22100-22106.

Lee S, Briklin O, Hiel H, Fuchs P. (2007) Calcium-dependent inactivation of calcium channels in cochlear hair cells of the chicken. J Physiol 583:909-922.

Lei D, Gao X, Perez P, Ohlemiller KK, Chen CC, Campbell KP, Hood AY, Bao J. (2011) Anti-epileptic drugs delay age-related loss of spiral ganglion neurons via T-type calcium channel. Hear Res 278:106-112.

Lopez I, Ishiyama G, Acuna D, Ishiyama A, Baloh RW. (2003) Immunolocalization of voltage-gated calcium channel alpha1 subunits in the chinchilla cochlea. Cell Tissue Res 313:177-186.

Marcotti W, Johnson SL, Holley MC, Kros CJ. (2003) Developmental changes in the expression of potassium currents of embryonic, neonatal and mature mouse inner hair cells. J Physiol 548:383-400.

Matar N, Jin W, Wrubel H, Hescheler J, Schneider T, Weiergraber M. (2009) Zonisamide block of cloned human T-type voltage-gated calcium channels. Epilepsy Res 83:224-234.

Mills JH, Matthews LJ, Lee FS, Dubno JR, Schulte BA, Weber PC. (1999) Gender-specific effects of drugs on hearing levels of older persons. Ann N Y Acad Sci 884:381-388.

Mizuta E, Shirai M, Arakawa K, Hidaka K, Miake J, Ninomiya H, Kato M, Shigemasa C, Shirayoshi Y, Hisatome I, Morisaki T. (2010) Different distribution of $Ca_v3.2$ and $Ca_v3.1$ transcripts encoding T-type Ca^{2+} channels in the embryonic heart of mice. Biomed Res 31:301-305.

Murphy MP, Gates GA. (1997) Hearing Loss: Does Gender Play a Role? Medscape Womens Health 2:2.

Nie L, Zhu J, Gratton MA, Liao A, Mu KJ, Nonner W, Richardson GP, Yamoah EN. (2008) Molecular identity and functional properties of a novel T-type Ca^{2+} channel cloned from the sensory epithelia of the mouse inner ear. J Neurophysiol 100:2287-2299.

Ohlemiller KK. (2006) Contributions of mouse models to understanding of age- and noise-related hearing loss. Brain Res 1091:89-102.

Pearson JD, Morrell CH, Gordon-Salant S, Brant LJ, Metter EJ, Klein LL, Fozard JL. (1995) Gender differences in a longitudinal study of age-associated hearing loss. J Acoust Soc Am 97:1196-1205.

Platzer J, Engel J, Schrott-Fischer A, Stephan K, Bova S, Chen H, Zheng H, Striessnig J. (2000) Congenital deafness and sinoatrial node dysfunction in mice lacking class D L-type Ca^{2+} channels. Cell 102:89-97.

Probst FJ, Corrigan RR, Del Gaudio D, Salinger AP, Lorenzo I, Gao SS, Chiu I, Xia A, Oghalai JS, Justice MJ. (2013) A point mutation in the gene for asparagine-linked glycosylation 10B (Alg10b) causes nonsyndromic hearing impairment in mice (Mus musculus). PLoS One 8e80408.

Rotschafer SE, Marshak S, Cramer KS. (2015) Deletion of Fmr1 alters function and synaptic inputs in the auditory brainstem. PLoS One 10e0117266.

Schacht J, Hawkins JE. (2005) Sketches of otohistory. Part 9: presby[a]cusis. Audiol Neurootol 10:243-247.

Scimemi P, Santarelli R, Selmo A, Mammano F. (2014) Auditory brainstem responses to clicks and tone bursts in C57 BL/6J mice. Acta Otorhinolaryngol Ital 34:264-271.

Shen H, Zhang B, Shin JH, Lei D, Du Y, Gao X, Wang Q, Ohlemiller KK, Piccirillo J, Bao J. (2007) Prophylactic and therapeutic functions of T-type calcium blockers against noise-induced hearing loss. Hear Res 226:52-60.

Simms BA, Zamponi GW. (2014) Neuronal voltage-gated calcium channels: structure, function, and dysfunction. Neuron 82:24-45.

So HS, Park C, Kim HJ, Lee JH, Park SY, Lee JH, Lee ZW, Kim HM, Kalinec F, Lim DJ, Park R. (2005) Protective effect of T-type calcium channel blocker flunarizine on cisplatin-induced death of auditory cells. Hear Res 204:127-139.

Spongr VP, Flood DG, Frisina RD, Salvi RJ. (1997) Quantitative measures of hair cell loss in CBA and C57BL/6 mice throughout their life spans. J Acoust Soc Am 101:3546-3553.

Tan HE, Lan NSR, Knuiman MW, Divitini ML, Swanepoel DW, Hunter M, Brennan-Jones CG, Hung J, Eikelboom RH, Santa Maria PL. (2018) Associations between cardiovascular disease and its risk factors with hearing loss-A cross-sectional analysis. Clin Otolaryngol 43:172-181.

Thuesen AD, Andersen K, Lyngso KS, Burton M, Brasch-Andersen C, Vanhoutte PM, Hansen PBL. (2018) Deletion of T-type calcium channels $Ca_v3.1$ or $Ca_v3.2$ attenuates endothelial dysfunction in aging mice. Pflugers Arch 470:355-365.

Tsubota M, Okawa Y, Irie Y, Maeda M, Ozaki T, Sekiguchi F, Ishikura H, Kawabata A. (2018) Involvement of the cystathionine-gamma-lyase/$Ca_v3.2$ pathway in substance P-induced bladder pain in the mouse, a model for nonulcerative bladder pain syndrome. Neuropharmacology 133:254-263.

Tucker-Davis Technologies . (2015) A Guide to ABR Testing with the System, 3, 2015RZ6.

Weiergräber M, Henry M, Südkamp M, de Vivie ER, Hescheler J, Schneider T. (2005) Ablation of Cav2.3 / E-type voltage-gated calcium channel results in cardiac arrhythmia and altered autonomic control within the murine cardiovascular system. Basic Res. Cardiol. 100(1):1-13.

Uemaetomari I, Tabuchi K, Nakamagoe M, Tanaka S, Murashita H, Hara A. (2009) L-type voltage-gated calcium channel is involved in the pathogenesis of acoustic injury in the cochlea. Tohoku J Exp Med 218:41-47.

Valderrama JT, de la Torre A, Alvarez I, Segura JC, Thornton AR, Sainz M, Vargas JL. (2014) Automatic quality assessment and peak identification of auditory brainstem responses with fitted parametric peaks. Comput Methods Prog Biomed 114:262-275.

Voisin T, Bourinet E, Lory P. (2016) Genetic alteration of the metal/redox modulation of $Ca_v3.2$ T-type calcium channel reveals its role in neuronal excitability. J Physiol 594:3561-3574.

Wang R, Lewin GR. (2011) The $Ca_v3.2$ T-type calcium channel regulates temporal coding in mouse mechanoreceptors. J Physiol 589:2229-2243.

Willott JF. (2001) Handbook of Mouse Auditory Research - From Behavior to Molecular Biology. CRC Press, 2001.

Xu W, Lipscombe D. (2001) Neuronal $Ca_v1.3$ alpha1 L-type channels activate at relatively hyperpolarized membrane potentials and are incompletely inhibited by dihydropyridines. J Neurosci 21:5944-5951.

Yeap LL, Lim KS, Lo YL, Bakar MZ, Tan CT. (2014) Valproate-induced reversible sensorineural hearing loss: a case report with serial audiometry and pharmacokinetic modelling during a valproate rechallenge. Epileptic Disord 16:375-379.

Yu YF, Wu WY, Xiao GS, Shi J, Ling HY. (2015) Effect of T-type calcium channel blockers on spiral ganglion neurons of aged C57BL/6J mice. Int J Clin Exp Med 8:15466-15473.

Yu YF, Wu WY, Xiao GS, Ling HY, Pan C. (2016) Protection of the cochlear hair cells in adult C57BL/6J mice by T-type calcium channel blockers. Exp Ther Med 11:1039-1044.

Zampini V, Johnson SL, Franz C, Lawrence ND, Munkner S, Engel J, Knipper M, Magistretti J, Masetto S, Marcotti W. (2010) Elementary properties of $Ca_v1.3$ Ca^{2+} channels expressed in mouse cochlear inner hair cells. J Physiol 588:187-199.

Zampini V, Johnson SL, Franz C, Knipper M, Holley MC, Magistretti J, Masetto S, Marcotti W. (2013) Burst activity and ultrafast activation kinetics of $Ca_v1.3$ Ca^{2+} channels support presynaptic activity in adult gerbil hair cell ribbon synapses. J Physiol 591:3811-3820.

Zamponi GW. (2016) Targeting voltage-gated calcium channels in neurological and psychiatric diseases. Nat Rev Drug Discov 15:19-34.

Zamponi GW. (2017) A Crash Course in Calcium Channels. ACS Chem Neurosci 8:2583-2585.

Zamponi GW, Lory P, Perez-Reyes E. (2010) Role of voltage-gated calcium channels in epilepsy. Pflugers Arch 460:395-403.

Zhang Y, Ji H, Wang J, Sun Y, Qian Z, Jiang X, Snutch TP, Sun Y, Tao J. (2018) Melatonin-mediated inhibition of $Ca_v3.2$ T-type Ca^{2+} channels induces sensory neuronal hypoexcitability through the novel protein kinase C-eta isoform. J Pineal Res 64(4)e12476.

(Received 26 August 2018, Accepted 12 April 2019)
(Available online 25 April 2019)